NTNU
Norwegian University of
Science and Technology

Experimental investigation of droplet breakage in the oil-in-water emulsion in a stirred tank

Seok Ki Moon

Chemical Engineering
Submission date: July 2018
Supervisor: Gisle Øye, IKP
Co-supervisor: Marcin Dudek, IKP

Norwegian University of Science and Technology
Department of Chemical Engineering

Summary

In the modern oil and gas industry, the amount of produced water becomes major issues as its production is increased, especially in the matured field. To dispose produced water to the sea or utilize it for re-injection process, a certain level of produced water quality needs to be achieved. To achieve its quality level, it is important to separate dispersed organic compounds out of the produced water. For the efficient separation of dispersed organic compounds, the oil-in-water emulsion droplet breakage phenomena are of fundamental interest and it was experimentally investigated in this thesis.

To investigate the emulsion droplet breakage phenomena, laser diffraction method and spinning drop method were used for measuring emulsion droplet size distribution and the interfacial tension between two phases. Silicone oil 50 and 100 with three different types of surfactants were used to examine their influence on the emulsion droplet breakage. As a continuous phase, MQ water, 0.1wt%, 3.5wt% and 20wt% NaCl solution were used for understanding its effect as well. The experiments were performed under the turbulent condition with purpose-built mixing tank and Rushton turbine.

Based on the experimental data, the influence of dispersed phase viscosity, different types of surfactants, salinity of continuous phase and dispersed phase volume fraction on the emulsion droplet size distribution was analyzed. Furthermore, the maximum size of the droplet in the emulsion was predicted by using Kolmogorov-Hinze theory and other advanced models in consideration with dispersed phase viscosity and the difference in mass density between the dispersed phase and the continuous phase. The comparison between the theoretical value of dv95 and dv95 values from the experiment was conducted to estimate the prediction capability of the model.

Acknowledgement

I would first like to thank my thesis supervisor Professor Gisle Øye. He consistently allowed this paper to be my own work, but steered me in the right the direction whenever he thought I needed it.

I would also like to thank Dr. Marcin Dudek as a co-supervisor of this thesis, and I am gratefully indebted to him for his very valuable comments on this thesis.

Finally, I must express my very profound gratitude to my parents for providing me with unfailing support and continuous encouragement throughout my years of study and through the process of researching and writing this thesis. This accomplishment would not have been possible without them.

Thank you.

Trondheim, 2018-07-26

Seok Ki Moon

Table of Contents

List of Tables

List of Figures

Chapter 1

Introduction

Petroleum reservoirs are referred to as structurally trapped formations that contain a large number of organic compounds and other by-products. During the production of oil and gas from these subsurface formations, those other by-products are also extracted simultaneously with targeted organic compounds. Among the other by-products, produced water(PW) is the largest by-product during oil and gas production in volume[23].

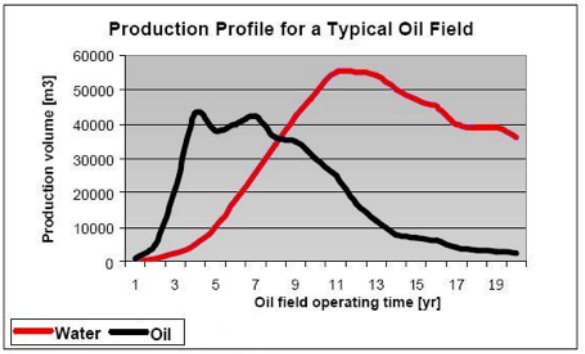

Figure 1.1: Production profile for a typical oil field [23]

It is well known that the amount of produced water from a typical oil field dramatically increases as the oil field matures. Production profile for a typical oil field is shown in

Figure 1.1. In some matured fields, produced water yields more than 90% of production fluid. Those produced water can be either re-injected into the formation for the purpose of recovery enhancement or discharged to the sea. But often, especially in the offshore oil field, produced water is mostly discharged to the sea. Figure 1.2 depicts that around 80% of produced water has been discharged to the sea in Norway and comparable amounts of produced water are forecasted to be disposed for the future as well. Figure 1.2 also illustrates an increasing amount of produced water re-injected.

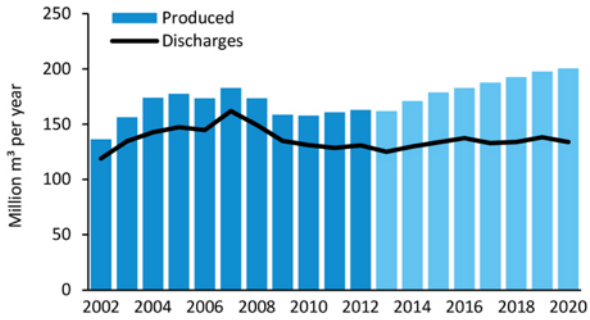

Figure 1.2: Historical volumes and forecasts for produced water and discharges[17]

To discharge to the sea or utilize for re-injection process, produced water should be treated properly to achieve a certain level of quality. Especially, dissolved or dispersed organic compounds need to be removed so that it is not environmentally harmful or does not cause any technical issues within the re-injection process. However, even after some treatment like hydrocyclone or gas flotation, they still exist within the produced water in the form of an oil-in-water emulsion. Therefore, the oil-water separation efficiency needs to be improved and oil-in-water emulsion droplet breakage and coalescence phenomena should be investigated thoroughly to enhance its separation process.

In principle, separation process of oil-in-water emulsion consists of several steps as illustrated in Figure1.3. Dispersed oil droplets move upward because of the density difference between continuous and dispersed phase. This process is called as creaming. In the meantime, gathered oil droplets get closer each other forming flocks, which is called

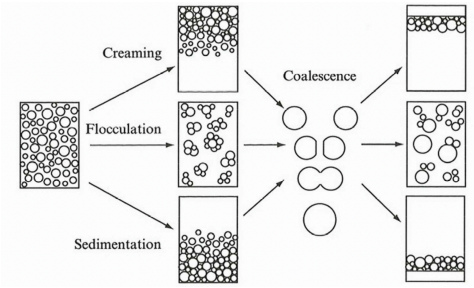

Figure 1.3: Steps of emulsion separation process

as flocculation process. After this, several oil droplets start to merge each other leading to the formation of a larger droplet. This process is referred to as coalescence and eventually, phase separation is followed by successive coalescence process. On the contrary, there is drop break-up process which happens in the opposite way of coalescence. Break-up process leads to the formation of several smaller drops from a larger one. Since oil-in-water emulsion is thermodynamically unstable and kinetically stable, the certain amount of energy is required to achieve drop break-up.

In real separation process system, fluid flow inside the process units is in a turbulent condition. This means that there is an energy input into the oil-in-water emulsion, promoting dispersed oil droplets to break-up. Thus, in reality, those two elementary processes, coalescence, and break-up are co-existing each other and it is directly related to the overall separation process efficiency. Therefore, to improve separation process efficiency, it is of fundamental interest to investigate factors affecting break-up and coalescence process of dispersed oil droplets in turbulent condition. The main problems are summarized as below:

1. **Dispersed oil droplets in produced water (oil-in-water emulsion)**
2. **Demand for separation process efficiency improvement**
3. **Co-existing two elementary processes in emulsion: break-up and coalescence**
4. **Consider turbulent condition as a real system**

The aim of this project is to investigate experimentally the formation of the oil-in-water emulsion under different mixing condition using purpose-built mixing setup. Specifically, the primary focus is to understand dispersed oil droplet breakage process under turbulent condition.

Chapter 2

Produced water

2.1 Produced water composition

Generally, the composition of produced water can be grouped into five different categories as follows[13]:

- **Dissolved and dispersed oil components**
- **Dissolved minerals**
- **Production chemicals**
- **Produced solids**
- **Dissolved gas**

Due to the different geological origins and the heterogeneity of reservoir formations, PW has a wide variation in its amount of each category. Specifically, dissolved and dispersed oil components are of the greatest concern in produced water due to its toxicity and negative impact on environment.[16, 29, 50]

Dissolved and dispersed oil components can be defined as a mixture of petroleum hydrocarbons. It mainly includes BTEX (benzene, toluene, ethylbenzene, and xylene), PAHs

(polyaromatic hydrocarbons) and phenols. BTEX is the most abundant hydrocarbons in produced water and has low molecular weight saturated hydrocarbons. PAHs consist of hydrocarbons containing two or more combined aromatic rings[29]. Different kinds of phenol derivatives, such as methylphenols, dimethylphenols, can also be found in produced water. Relatively polar organic compounds and smaller molecules in size (molecular weight) are more likely to be present in dissolved oil components than dispersed oil components, which are oil droplets.

In dispersed oil droplets, most of the saturated hydrocarbons are existing because of its low solubility. It has been reported that the shorter chain alkanes(ranging from the carbon number of 10 to 22) are more abundant than the longer chain alkanes[29]. For the same reason, a great part of PAHs and alkyphenols are associated with dispersed oil droplets in high conentration[14, 25]. Both components are known as highly toxic substances for marine eco-system. Particularly, PAHs are of the greatest environmental concern in produced water because of their persistence in the marine environment[36]. Thus, it can be described that dispersed oil components contain more environmentally detrimental substance than dissolved components in terms of their volume within the produced water and their concentration of each oil droplets. Hence, negative impacts on the environment from dispersed oil components are prevailing compared with other composition of produced water and accordingly, many efforts have been invested to regulate the discharge amount of dispersed oil components in produced water around the world.

2.2 Environmental legislation

In past, general legislation of dispersed oil droplet concentration in produced water has been 40ppm to be able to discharge to the sea[23]. The Convention for the Protection of the Marine Environment of the North-East Atlantic (OSPAR) agreed to reduce the maximum discharge limit of dispersed oil in produced water at 30ppm and the overall discharges in produced water by 15% from 1999 level[34]. According to the United States Environ-

Country / Organization	Monthly Average Limit (mg/L)	Daily Average Limit (mg/L)
Canada	30	60
USA	29	42
OSPAR (NE Atlantic)	30	-
HELCOM	15	-
Mediterranean Sea	40	100
China	10	100
Western Australia	30	50
Nigeria	40	72
Brazil	-	20
Kuwait	40	100

Table 2.1: Monthly and daily average concentration(mg/L) limit permitted by several countries of total dispersed oil in produced water for discharge to sea[29, 49]

mental Protection Agency (USEPA), daily maximum concentration limit of oil and grease in produced water is 42ppm and the monthly average limit is 29ppm[46]. In Australia, allowed oil and grease limits for treated produced water discharge offshore are 50ppm instantaneous and 30ppm for daily average[36]. The People's Republic of China sets the monthly average limits of oil and grease discharge at 10ppm[44]. In 2000, the EU Water Framework Directive (WFD) was adopted which is committed to 'zero discharge' in compliance with the need for a more protective system to prevent aquatic pollution[11]. The oil operators in Norway have agreed to implement zero environmental harmful discharge policy within 2005. For this, Pollution Control Authority (SFT) and The Norwegian Industries Associations (OLF) have developed the Environmental Impact Factor (EIF) to achieve the zero harmful discharge strategy[34]. Likewise, OSPAR commision has also agreed on the policy of zero discharge of pollutants into the sea[8]. Therefore, one can conclude that most of oil and gas companies as well as the governments around the world are currently working towards the implementation of '*zero-discharge*' of contaminants or pollutants in produced water.

2.3 Produced water treatment

In onder to discharge the produced water to the sea or re-inject into the formation, certain level of produced water quality should be accomplished to meet the environmental regulations. To achieve this requirement, proper treatment is necessary to separate the dispersed oil components out from the produced water.

Typically, three types of separation unit are commonly and widely used in oil and gas production process as shown in below Figure2.1. Separated produced water after three-

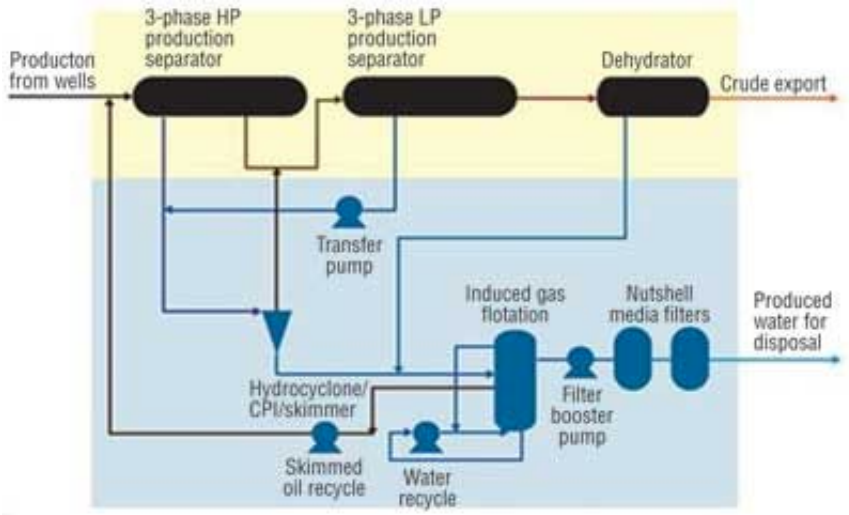

Figure 2.1: Typical produced water treatment pakage

phase gravity separator, however, includes a large number of impurities that need to be removed, forming the oil-in-water emulsion. Subsequent hydrocylcone and gas flotation units are employed to get rid of those remaining oil droplets in produced water. Since there is no treatment process that is 100% effective, treated produced water is still containing some dispersed oil droplets. According to the 2014 OSPAR discharges data, the annual concentration of dispersed oil in discharged produced water in Norway was 12.5ppm[38]. It has been also reported that the size of remaining dispersed oil droplets in produced water after treatment is ranging from 1 to 10μm[25]. Therefore, in order to achieve the

'*zero-discharge*' goal, it is obvious that separation process efficiency needs to be more improved.

Chapter 3

Basic Theory

3.1 Droplet breakage

An emulsion is defined as a mixture of two or more immiscible fluids. Produced water is regarded as oil-in-water emulsion since remaining oil droplets are dispersed in water. In this case, water is the continuous phase and oil droplets are dispersed phase.

Produced water is thermodynamically unstable, but kinetically stable emulsion. This means that there is no spontaneous formation of dispersion and immediate phase separation will occur. Therefore, because of the density difference between continuous and dispersed phase, dispersed oil droplets will move upward and finally be separated by coalescencing into an oil film on top. However, in a turbulent condition, a certain amount of energy is introduced into the emulsion. This energy input, which is a hydrodynamic force, stabilizes emulsion by breaking up dispersed oil droplets and inhibits emulsion from phase separation. Hence, drop break-up process contributes to emulsion stability, while the coalescence process is responsible for emulsion destabilization and phase separation. In produced water system, which is the oil-in-water emulsion system, those two opposite fundamental processes shown in Figure 3.1 are co-existing in turbulent condition.

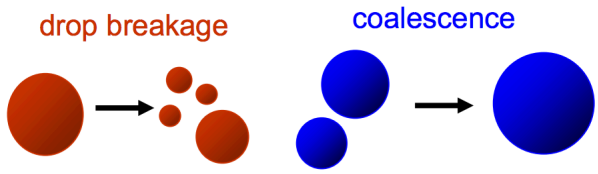

Figure 3.1: Illustration of drop break-up and coalescence processes

3.1.1 Droplet break-up mechanism

In turbulent condition, the kinetic energy of the turbulent motion in the continuous phase brings about the break-up of the dispersed oil droplet[21]. When the kinetic energy is exerted on a droplet, it starts to deform in various ways. Generally, at first, a single droplet is stretched as shown in Figure 3.2. Then, it may show a binary break-up as shown in Figure 3.2(b), but in most cases, secondary small droplets are formed as illustrated in Figure 3.2(a).

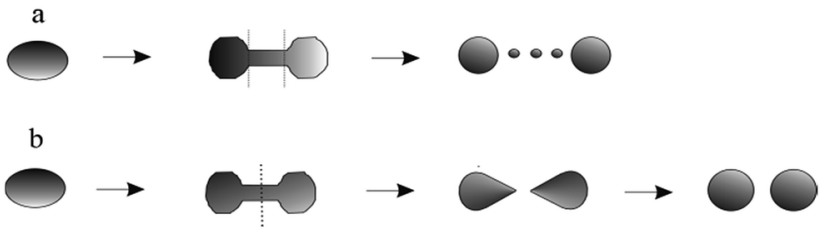

Figure 3.2: Examples of single droplet break-up pattern

For characterization of droplet break-up in turbulent, the interaction between the hydrodynamic force from turbulence and interfacial tension of droplet plays a major role. The relationship between hydrodynamic force and interfacial tension can be expressed in one dimensionless number which is called as '*Weber number*'[30]. The dimensionless Weber Number represents the ratio of disruptive hydrodynamic forces to the stabilizing interfacial tension force as expressed in Equation 3.1. Therefore, it shows whether the kinetic or the interfacial tension energy is dominant. The Weber number is written as:

$$We = \frac{\rho v^2 l}{\sigma} \tag{3.1}$$

where ρ is the density of the fluid, v is fluid velocity, l is a fluid characteristic length which is typically the droplet diameter and σ is the interfacial tension.

Systematic experimental investigation on a single droplet break-up in stirred liquid-liquid tank has been performed by Solsvik et al[41]. Several kinds of droplet break-up pattern were observed with different kinds of dispersed phase as shown in below Figure 3.3, 3.4, 3.5.

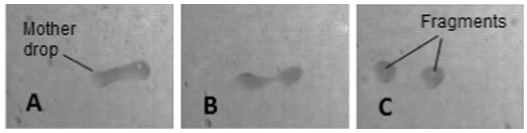

Figure 3.3: Equally sized binary break-up of a single droplet, petroleum-in-water system. [41]

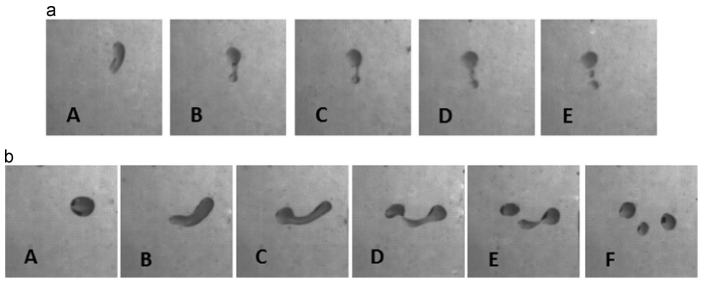

Figure 3.4: Ternary break-up of a single droplet, toluene-in-water.[41]

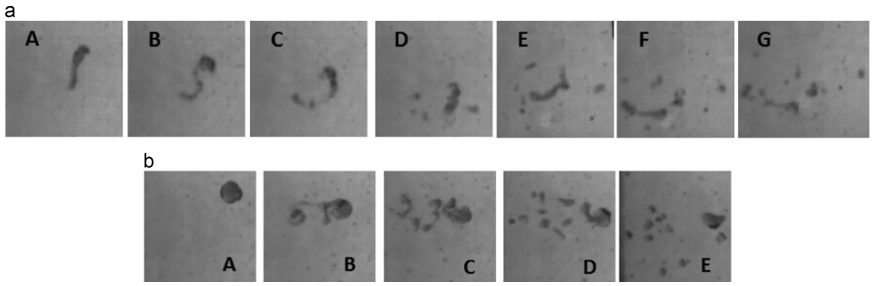

Figure 3.5: Multiple break-up of a single droplet,toluene-in-water.[41]

According to their research, it was revealed that unequal-sized break-up is more dominant rather than equal-size break-up. Also, multiple break-up events were more commonly observed than binary break-up, and its possibility increased with the size of mother drop. Oppositely, mother drops with smaller size tend to produce binary break-up events.

3.2 Emulsification in turbulent flow

Droplet break-up and coalescence are two fundamental processes consisting of emulsification. During the emulsification process, these two opposite processes compete with each other and drop-size distribution is evolving[9, 45]. Along with the drop size, the size of eddies created in turbulent is used to classify the regime of emulsion in turbulent condition.

3.2.1 Emulsification flow regime

There are two different regimes of emulsification which are termed as '*turbulent inertial regime*' and '*turbulent viscous regime*' respectively. Schematic presentation of each regime is illustrated in Figure3.6. In turbulent inertial regime, drops are larger in diameter than the smallest turbulent eddies in the continuous phase. On the other hand, in turbulent viscous regime, drop diameter is smaller than the size of the smallest eddies. The transition regime exists in between two regimes and also depends on the maximum size of drop and smallest eddies in turbulent condition[47]. The size of the smallest eddies in turbulent, λ_0, is given by '*Kolmogorov scale*' as follows[26]:

$$\lambda_0 \approx \varepsilon^{-\frac{1}{4}} \eta_C^{\frac{3}{4}} \rho_C^{-\frac{3}{4}} \tag{3.2}$$

where ε is energy dissipation rate per unit mass of the fluid, η_C and ρ_C are dynamic viscosity and mass density of continuous phase respectively.

(a) Turbulent inertial regime **(b)** Turbulent viscous regime

Figure 3.6: Schematic presentation of two different regime[47]

3.2.2 Energy dissipation rate

The experimental matrix involved changing the mixing speed during the emulsification. There were three factors that limited the impeller rotation speed range.

The primary factor was Reynolds number which determines the fluid flow regime in the mixing tank. Reynolds number in the mixing tank can be calculated as below[24]:

$$Re = \frac{\rho N D^2}{\mu} \tag{3.3}$$

where ρ is mass density of the liquid in the tank, N is mixing speed in RPM, D is a diameter of the impeller and μ is the dynamic viscosity of the liquid. If Reynolds number is larger than 1000, then fluid flow is regarded as turbulent. Therefore, the minimum required impeller rotation speed for turbulent flow can be calculated at Reynolds number of 1000.

However, creaming of crude oil on the liquid surface was observed with the calculated minimum required impeller rotation speed. Creaming of dispersed phase indicates that both continuous phase and dispersed phase are not properly mixed leading to failure of emulsification in turbulent. Therefore, appropriate impeller rotation speed was needed to be found by hand.

For higher impeller rotation speed, air bubbles were generated in the liquid and showed a tendency to stay within mixing flow. Air bubbles inhibited obtaining accurate drop size distribution data, because of oil-covered air bubbles. These oil-covered air bubbles were

detected as oil droplets, resulting in significant distortion of drop size distribution data. Thus, the maximum available impeller rotation speed with no air bubbles was also determined by hand. In this experiment with Rushton turbine, it was around 1150RPM.

Therefore, within the applicable mixing speed range, the evolution of silicone oil droplet size distribution was investigated experimentally in relation with average energy dissipation rate. The average energy dissipation rate can be expressed as below equation[41]:

$$\overline{\varepsilon} = \frac{P}{\rho V} \tag{3.4}$$

where ρ is mass density of the liquid in tank and V is the volume of the liquid in tank. P is power comsumption, which is given by[24]:

$$P = N_p \rho N^3 D^5 \tag{3.5}$$

where N_p is the dimensionless Newton number, ρ is mass density of the liquid in tank, N is mixing speed in RPM and D is diameter of impeller. There are numerous ways to approximate N_p, but value of 5.75 is widely utilized value for six-blade open impeller[37, 41].

3.2.3 Maximum drop diameter

The maximum size and/or diameter of a drop is an important parameter because it is the largest drop size that can resist the nearby disruptive forces of the flow[21]. Thus, in turbulent inertial regime, maximum drop diameter is determined by the balance between the fluctuations in the hydrodynamic pressure of the continuous phase and drop capillary pressure. In case of turbulent viscous regime, maximum drop diameter is determined by the balance between the viscous stress acting from the continuous phase on the drop surface and the drop capillary pressure[47, 48]. Since produced water is very a diluted oil-in-water emulsion, it is relevant to the turbulent inertial regime.

By the importance of maximum drop diameter during emulsification, notable attempts have been introduced to predict maximum drop size.

Under the assumption of the not too small value of *Reynolds number*, Weber number was used to analyze droplet break-up by Hinze[21]:

$$(N_{We})_{crit} = \frac{\rho_C \overline{v^2} D_{max}}{\sigma} \tag{3.6}$$

where $(N_{We})_{crit}$ is critical value of Weber number for break-up, ρ_C is mass density of the continuous phase, $\overline{v^2}$ is mean square of velocity over a distance at D_{max}, D_{max} is maximum drop diameter and σ is interfacial tension.

This expression was related to an isotropic homogeneous turbulence. Several investigations showed that mean square turbulent velocity fluctuations are typical of the order of the energy dissipation rate times the length scale under consideration to the power $\frac{2}{3}$[2, 27]:

$$\overline{v^2} = C_1(\varepsilon D)^{\frac{2}{3}} \tag{3.7}$$

where C_1 is numerical constant and $C_1 \simeq 2.0$ by Batchelor[1].

Substitute Equation3.7 into Equation3.6, following expression for D_{max} was derived:

$$D_{max} = A_1 \varepsilon^{-\frac{2}{5}} \sigma^{\frac{3}{5}} \rho_C^{-\frac{3}{5}} \tag{3.8}$$

where A_1 is a proportional constant of the order of unity, ε is energy dissipation rate per unit mass of the fluid, σ is interfacial tension and ρ_C is mass density of the continuous phase[47]. This is generally referred to as '*Kolmogorov-Hinze theory of emulsification*'. This has been verified and modified in several studies later[5, 7, 40, 42, 53].

However, the influence of dispersed phase viscosity was not taken into account in Kolmogorov-Hinze theory of emulsification. It is only valid for dispersed phase with relatively low viscosity, similar to that of water[47]. Thus their approach was modified for

more viscous dispersed phase by Davies[10] and Calabrese et al.[6] as following equation:

$$D_{Max} = A_2(1 + A_3\frac{\eta_D\varepsilon^{\frac{1}{3}}D_{Max}^{\frac{1}{3}}}{\sigma})^{\frac{3}{5}}\sigma^{\frac{3}{5}}\rho_C^{-\frac{3}{5}}\varepsilon^{-\frac{2}{5}} \tag{3.9}$$

where A_2 and A_3 are numerical constants, η_D is dynamic viscosity of dispersed phase. When η_D goes to 0, the influence of dispersed phase viscosity disappears and then the Equation3.9 is simplified to the Equation3.8.

Above derived equation, however, does not consider the difference of the mass density between continuous phase and dispersed phase. It is valid only for the emulsion which has similar mass density difference between continuous phase and dispersed phase. By taking into account the density difference, below equation was derived[4, 54]:

$$D_{Max} = A_4(1 + A_5(\frac{\rho_C}{\rho_D})\frac{\eta_D\varepsilon^{\frac{1}{3}}D_{Max}^{\frac{1}{3}}}{\sigma})^{\frac{3}{5}}\sigma^{\frac{3}{5}}\rho_C^{-\frac{3}{5}}\varepsilon^{-\frac{2}{5}} \tag{3.10}$$

where A_4 and A_5 are numerical constants, ρ_D is the mass density of dispersed phase. When $\rho_C = \rho_D$, the effect of density difference between continuous phase and dispersed phase disappears and the Equation3.10 is simplified to the Equation3.9. Since $\rho_C \approx \rho_D$ in most cases, the numerical constants in Equation3.9 and Equation3.10 are correlated each other. The numerical constant A_2 in Equation3.9 and A_4 in Equation3.10 are related to the effect of the capillary pressure, while A_3 in Equation3.9 and A_5 in Equation3.10 are related to the effect of the drop viscosity[47]. The value of numerical constants are different in different experimental system and materials.

Further development of equation was conducted experimentally by Lagisetty et al.[28] for non-Newtonian fluid. Since both the continuous phase and dispersed phase in this project are the Newtonian fluid, the equations derived by Lagisetty et al.[28] will not be reproduced in this report.

Chapter 4

Experiment

4.1 Method

4.1.1 Laser diffraction method

Drop size distribution of prepared emulsion was measured by a laser diffraction method. Specifically, Mastersizer 3000(product of Malvern Instrument, UK) was used to measure the size of the dispersed oil droplet within the continuous phase. In principle, by taking advantage of the laser diffraction method, drop size distribution was measured by quantifying the intensity of scattered light as the laser beam passes through emulsion containing dispersed oil droplets. The scattered light has angular variation depends on the size of the dispersed droplet. Simple illustration on light scattering method principle is described in Figure 4.1.

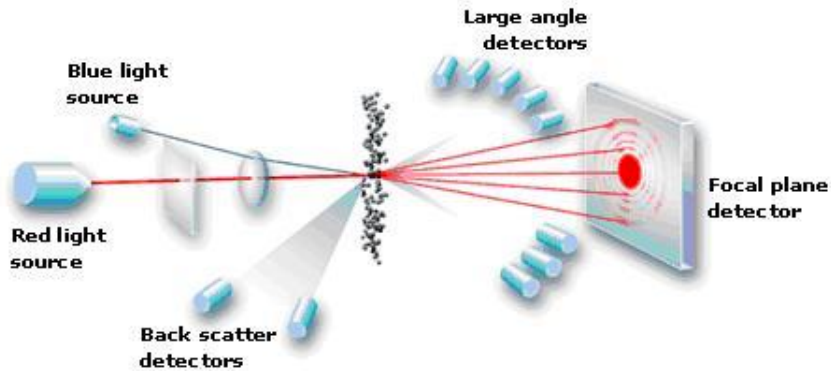

Figure 4.1: Principle of light scattering method

When the dispersed droplet is large, then the light is scattered in small angles. On the contrary to this, when the dispersed droplet is small, then the light is scattered in a large angle. By detecting angular scattered light and analyzing its intensity, the size of dispersed oil droplets can be calculated using the '*Mie theory*' of light scattering. Previously, Mie theory has been used to measure oil concentration in water, which is oil-in-water emulsion[19, 31].

Mie theory is primarily based on Maxwell's electromagnetic field equations and estimates the intensity of scattered light induced by all dispersed objects, whether they are transparent or opaque. The theory is based on following assumptions[32]:

1. The dispersed droplets are spherical
2. The emulsion is dilute; scattered light from one droplet is not disturbed by other droplets
3. The optical properties of droplets are known, e.g. refractive index
4. The dispersed droplets are homogeneous

Based on the above assumptions, the optical properties of both the continuous phase and dispersed phase are required to obtain the accurate size of dispersed droplets in the emulsion. Here, the optical property indicates the refractive index of materials. Thus, the

refractive index of all samples was measured by refractometer before measuring drop size distribution. Though the basic assumptions of Mie theory are somewhat idealized, it is still a widely used problem-solving method for sizing dispersed droplets.

4.1.2 Spinning drop method

For measuring interfacial tensions, the spinning drop method was used (spinning drop tensiometer, SVT 20, DataPhysics Instruments GmbH). Here, a silicone oil drop is located in the middle of a glass tube filled with a higher density liquid, which rotates around its own axis with a constant angular velocity (ω [s^{-1}]) [12]. As the acceleration force by rotation gets high, the gravity force gets negligible and the drop stays a stable position in the center of the rotating tube (Figure 4.2) [33]. Provided gyrostatic equilibrium inside the tube, the shape of the drop provides a reliable and precise measurement of the interfacial tension between both phases.

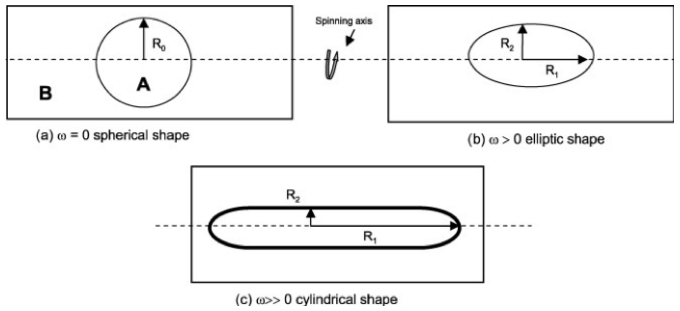

Figure 4.2: Spinning drop method [51]

Below Equation 4.1, gives the interfacial tension as a function of R and the density difference between both fluid phases [52].

$$\gamma = \frac{1}{4}\Delta\rho\omega^2 R^3 \tag{4.1}$$

where γ is the interfacial tension, $\Delta\rho$ is the density difference between phase, ω is the angular velocity and R is the cylinder radius.

4.2 Material

All materials and chemicals used in this work were obtained from appropriate suppliers. Below is some general information about the major materials in this work.

4.2.1 Silicone oil

As a dispersed phase, silicone oil was used for this experiment. The general chemical structure of silicone oil is depicted in Figure 4.3.

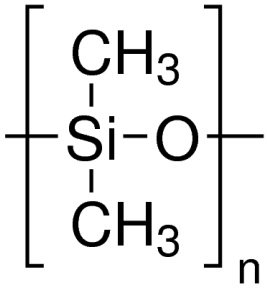

Figure 4.3: Chemical structure of silicone oil

Silicone oil is polymerized siloxane with organic side chain which is transparent liquid oil. The density of silicone oil is 0.96 g/ml at $25\,^{\circ}\mathrm{C}$ and the refractive index is 1.403. Both the density and refractive index of silicone oil were given by the supplier.

In this work, two different types of silicone oil were used, which are silicone oil 50 and silicone oil 100. The only difference between these two is viscosity. The viscosity of silicone oil 50 is 47.95 $mPa \cdot s$ and the viscosity of silicone oil 100 is 95.9 $mPa \cdot s$ at $25\,^{\circ}\mathrm{C}$. The viscosity of silicone oil 50 and silicone oil 100 was provided by the supplier.

In this experiment, silicone oil was selected as a dispersed phase for several reasons. First, the density of silicone oil is comparable to the density of the water and 3.5wt% NaCl brine. This was necessary to prevent creaming under turbulent mixing. Another reason for choosing silicone oil is because of its homogeneousness. Therefore, a chemical induced error could be minimized during the experiment.

4.2.2 Sodium dodecylbenzene sulfonate (SDBS)

In this experiment, sodium dodecylbenzene sulfonate (SDBS; MW = 348.48 g/mol) was used as anionic surfactant soluble in water. The general structure of SDBS is depicted in Figure 4.4.

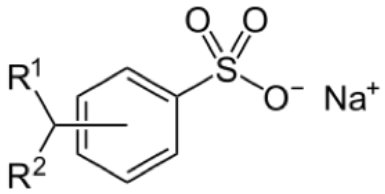

Figure 4.4: General structure of sodium dodecylbenzene sulfonate surfactants.

SDBS is a conventional amphiphile with one non-polar tail and one hydrophilic head group and involved in the group of alkylbenzene sulfonates. Like typical alkylbenzene sulfonates, SDBS is consist of different isomers, where the location of the alkyl chain at the aromatic ring can vary.

In contrary to AOT, SDBS does not tend to form microemulsion without co-surfactant. [39].

4.2.3 Sodium *bis*(2-ethylhexyl) sulfosuccinate (AOT)

Sodium *bis*(2-ethylhexyl) sulfosuccinate (AOT; MW = 444.56 g/mol) is another water soluble anionic surfactant that was used in this experiment. The chemical structure of AOT is illustrated in Figure 4.5.

Because of its double tailed structure, AOT has large packing parameters and tend to form large aggregates, such as lamellar phases and reversed micelles [15, 55, 18].

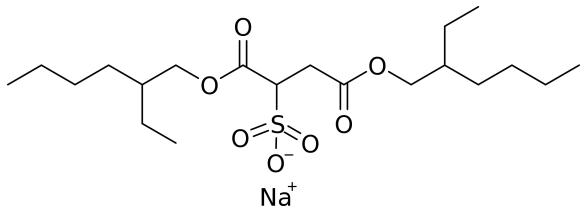

Figure 4.5: Chemical structure of sodium *bis*(2-ethylhexyl) sulfosuccinate (AOT)

AOT has a strong tendency to adsorb at the hydrocarbon-water interface and is capable of reducing the interfacial tension by several orders in magnitude[35, 20]. This is closely related to its capability to form microemulsions of all three Winsor types as a function of electrolyte concentration with no co-solvents or co-surfactants [3, 35].

4.2.4 Span® 80

Non-ionic, oil soluble surfactant, span® 80 (MW = 428.60 g/mol) was used in this experiment as well. The general structure of Span® 80 is shown in Figure 4.6.

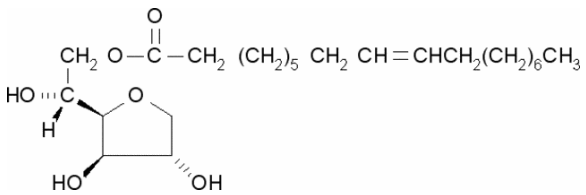

Figure 4.6: Chemical structure of Span® 80

The Span® 80 tail is composed of the alkyl group of fatty acid. It exists in a form of very viscous liquid and is soluble in non-polar material such as silicone oil.

Span® 80 is stable in mild acids, alkali, and electrolytes and do not react with ionic ingredients or actives. It functions as a non-ionic emulsifier and co-emulsifier. Also, it is stable over a wide range of pH.

4.3 Experimental setup

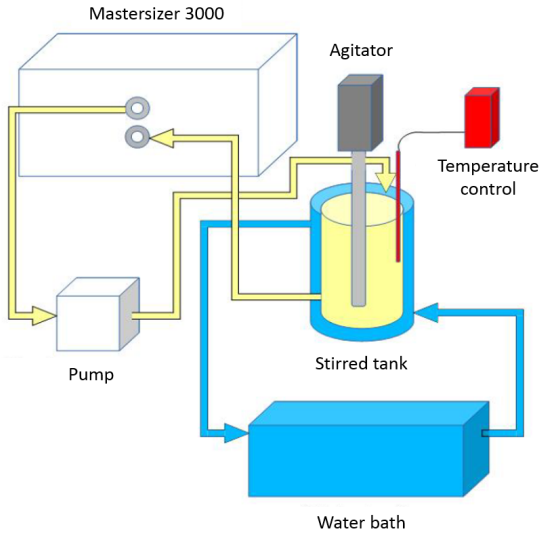

Figure 4.7: Schematic illustration of experimental setup for drop size distribution measurement

Figure 4.7 depicts the experimental setup for emulsion drop size distribution measurement. Primarily, this setup consists of four major parts which are mixing, measurement, circulation and temperature control.

4.3.1 Mixing

To be able to make the oil-in-water emulsion in turbulent condition, four-baffled mixing tank and impeller with a stirrer were used. As a stirrer, EUROSTAR digital(product of IKA, Germany), which has a capacity of rotation speed range from 50RPM to 2000RPM, was used to prepare the emulsion. In accordance with the stirrer, various kinds of impellers were tested and finally, the Rushton turbine was chosen for the main experiment.

Adopted turbine for the experiment is a disk-type radial impeller with six blades on it, the so-called 'Rushton turbine'. As a radial-type impeller, it tends to pump fluid upward or downward while discharging radially. It tends to pump in a more radial direction than

axial-flow impeller. Since it has disk geometry in the middle of the blade, it provides more uniform radial flow pattern and draws more power than open impeller[37].

The mixing tank is also a purpose-built double-layer glass tank with four off-the-wall baffles inside. Double-layer glass tank was chosen to control the emulsion temperature by circulating water in between the inner layer and outer layer.

The most important part of the mixing tank is baffles. Baffles are plates attached to the tank inner wall to disturb or redirect the flow. They are installed the inner wall of the tank to avoid solid body rotation and central vortex flow[24, 43]. The solid body rotation and central vortex flow pattern is illustrated in Figure 4.8. In solid body rotation, the fluid acts as if it were a solid mass resulting in little mixing. Central vortex flow often takes place at high impeller rotation speed without baffles in tank. Once it is formed, due to the centrifugal forces, the impeller pushes the fluid out to the walls. In some cases, the surface vortex reaches to the impeller blades, causing air entrainment[43].

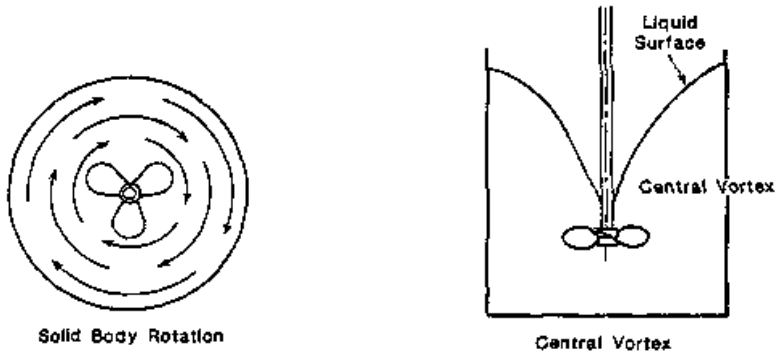

(a) Illustration of solid body rotation **(b)** Illustration of central vortex

Figure 4.8: Flow pattern without baffle in mixing tank[43]

Therefore, four-baffled mixing tank was adopted for this experiment. Baffles were attached on the wall using glue. The space between tank bottom and baffles were left intentionally to prevent unexpected accumulation by the formation of dead zone during turbulent mixing.

4.3.2 Circulation

For continuous measurement of drop size distribution, emulsion flow circulation is essential for the entire system. For this reason, a diaphragm pump(LIQUIPORT NF 300, product of KNF, Germany) was used. When measuring drop size distribution, low pumping rate was preferred, because the air bubbles were created while fluids were passing through the pump. The generated air bubbles distorted the drop size distribution data since Mastersizer3000 detected an oil-covered air bubble as an oil droplet. Therefore, the lowest possible pumping rate was chosen for all sets of experiments. The flow rate used in this experiment was approximately $700 mL/min$.

4.3.3 Temperature control

During the measurement, the emulsion temperature was maintained at $25\,^{\circ}\mathrm{C}$. The water bath (Ministat cc1, product of HUBER, USA) was used to control the entire system temperature. For monitoring, digital thermometer(product of VWR, USA) was used. Water was circulated through inter-layer of glass mixing tank by water bath and adjusted manually by monitoring temperature on thermometer.

4.3.4 System configuration

The experimental description is summarized in Table 4.1. Impeller was connected to stirrer and its blades were located at one-third point of liquid height from the tank bottom. The inlet of Mastersizer3000 measuring cell is directly connected to the emulsion inside the mixing tank by tubing, thus sample passing through the measuring cell has not interfered before measurement. The outlet of Mastersizer3000 measuring cell was connected directly to the inlet of the diaphragm pump by 5mm diameter polyethylene tubing to drain measured sample out from the Mastersizer3000 measuring cell. Finally, the outlet of the diaphragm pump was also linked straight by tubing to the emulsion inside the mixing tank for circulating sample. The inlet and outlet position of sampling had little

influence on measured data. Thus, they were located right next to the impeller blade where the largest turbulent energy dissipation was expected.

Number of baffles	(off-the-wall)	4
Width of baffles	(cm)	0.9
Number of impeller blades		6
Impeller location (from bottom)	(cm)	3.6
Impeller power number		5.75
Temperature	(°C)	25
Diameter of impeller	(cm)	3.6
Diameter of tank	(cm)	10.8

Table 4.1: Describtion of experimental system

In the meantime, the water bath was connected to the double-layer glass mixing tank for the purpose of temperature control. Temperature-controlled water was injected into the inter-layer inlet, which is located at the bottom of the glass mixing tank. When the inter-layer of glass mixing tank was completely filled with water, it flew back to the water bath through the inter-layer outlet located at the top of the glass mixing tank. Thus, it formed circulation of water, controlling emulsion temperature same as the water temperature. The real-time temperature of the emulsion was monitored by putting digital thermometer probe directly into the emulsion.

A lid made up of teflon was closing at the top of the glass mixing tank all the time during the experiment to avoid the accidental splash of the emulsion to outside.

Chapter 5

Result

5.1 Interfacial tension

Interfacial tension of silicone oil 50 with different surfactants and concentration were measured by using a spinning drop method. Below Figure 5.1 shows the interfacial tension trend according to the surfactants concentration and the exact values are also shown in Table 5.1 and 5.2. The interfacial tension shows a decreasing trend when the concentration of surfactants is increasing. Therefore, it is obvious to say that the more surfactants exist within the phase, the less interfacial tension values observed.

Interfacial tension is very important physicochemical property in terms of the size of emulsion droplet. Since interfacial tension is a fundamental property that explains about the interface between two different phase, it is deeply involved in the droplet break-up and coalescence phenomena. Therefore, it plays a major role when it comes to the emulsion droplet size distribution, as well as the prediction of maximum droplet size in the emulsion.

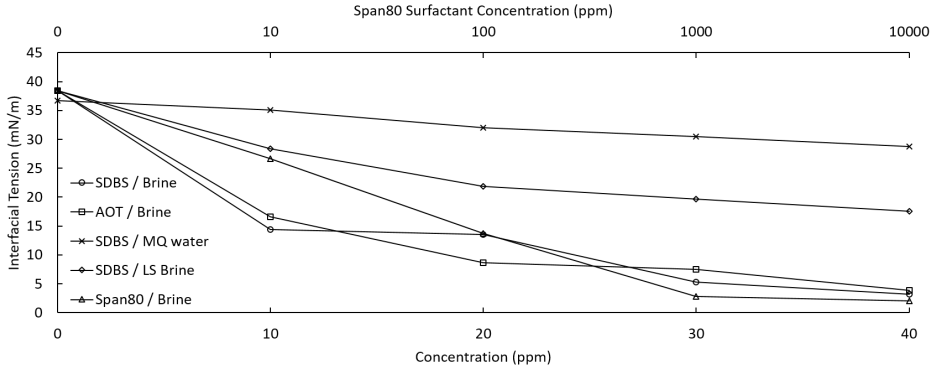

Figure 5.1: Interfacial tension of silicone oil 50 with different surfactants and concentration

Concentration (ppm)	SDBS with brine (mN/m)	AOT with brine (mN/m)
0	38.4	38.4
10	14.4	16.6
20	13.5	8.6
30	5.3	7.5
40	3.2	3.9
Concentration (ppm)	SDBS with MQ water (mN/m)	SDBS with LS brine (mN/m)
0	36.7	38.4
10	35.1	28.4
20	32	21.9
30	30.5	19.7
40	28.8	17.6

Table 5.1: Interfacial tension of silicone oil 50 with different kinds of surfactants and concentrations

Concentration (ppm)	Span® 80 (mN/m)
0ppm	38.4
10ppm	26.7
100ppm	13.7
1000ppm	2..8

Table 5.2: Interfacial tension of silicone oil 50 with different concentration of Span® 80

As shown in above tables, the concentration of surfactants varies from 10ppm to 40ppm except for the Span® 80 surfactant. This was determined by conducting several measurements to find a reasonable range of interfacial tension. Therefore, the minimum value of interfacial tension was around 3mN/m, which is very low. On the other hand, the concentration of Span® 80 surfactants was determined within the range of 10ppm to 1000ppm. Since Span® 80 surfactants exist in a very viscous liquid form, it was very difficult to measure the exact amount of surfactant. Also, since it is diluted into the silicone oil 50, it requires a large amount of silicone oil 50 sample to make the lower concentration of Span® 80 solutions. But, it still provides a reasonable range of interfacial tension values, Span® 80 concentration of 10, 100 and 1000ppm were adopted in this experiment.

5.2 Droplet size distribution

In the droplet size distribution measurement, four different variables were considered. These are dispersed phase viscosity, interfacial tension, continuous phase salinity and dispersed phase volume fraction. Viscosity was manipulated by using silicone oil 50 and silicone oil 100. These are different only in viscosity, and every other property is the same. Interfacial tension between the dispersed phase and continuous phase was controlled by

using different kinds of surfactant and their concentration. Except for the Span 80 surfactant, the concentration of surfactant varies from 0 to 40ppm with a step size of 10ppm. The concentration of Span 80 surfactant is determined as 10, 100 and 1000ppm due to the technical reasons. Deionized water, low and high salinity water are also used to investigate the effect of electrostatic force. Furthermore, the dispersed phase volume fraction is also changed to investigate its effect. Below Table 5.3 shows the entire set of experiment.

Type of silicone oil	Type of surfactant	Continuous phase	Dispersed phase volume fraction (v/v)
Silicone oil 50	SDBS	3.5wt% NaCl brine	0.5%
Silicone oil 100	SDBS	3.5wt% NaCl brine	0.5%
Silicone oil 50	AOT	3.5wt% NaCl brine	0.5%
Silicone oil 50	Span® 80*	3.5wt% NaCl brine	0.5%
Silicone oil 50	SDBS	MQ water	0.5%
Silicone oil 50	SDBS	0.1wt% NaCl brine	0.5%
Silicone oil 50	SDBS	25wt% NaCl brine	0.5%
Silicone oil 50	SDBS	3.5wt% NaCl brine	0.1%
Silicone oil 50	SDBS	3.5wt% NaCl brine	1%

Table 5.3: List of the experiments conducted with surfactant concentration of 10, 20, 30, 40 ppm
*Only Span® 80 concentration is different with other surfactant (10, 100, 1000ppm)

Other conditions such as rotation speed, temperature are maintained as same. Also, purpose-built Rushton turbine and 4 off-the-wall baffled mixing tank were used for all experiments as shown in Table 5.4.

Rotation Speed (RPM)	Temperature(°C)	Impeller type	Mixing tank
1150	25	6-blade rushton turbine	4 off-the-wall baffled mixing tank

Table 5.4: Other experiment conditions

During the experiment, the droplet size distribution was measured in volume distribution which is very common in laser diffraction method. The initial point of droplet size distribution means the point right after the sample input was completed. And the concentration represents the concentration of the surfactant.

Each of the droplet size distribution curve corresponding to the surfactant concentration was determined when it reaches to the steady-state point. In this case, the steady state point indicates the point that there are very little variations in droplet size distribution. This was determined by observing dv95, dv90, dv50 and dv10 values continuously. Figure 5.2 illustrates the concept of dv values.

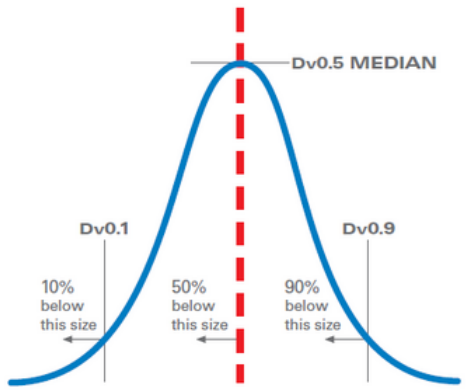

Figure 5.2: Concept of dv values in size distribution [22]

5.2.1 Dispersed phase viscosity

Droplet size distribution of emulsion with two different dispersed phase viscosity was investigated. It was conducted by using silicone oil 50 and silicone oil 100, which are different only in the viscosity. Other conditions like type of surfactant, continuous phase and dispersed volume fraction are maintained as same.

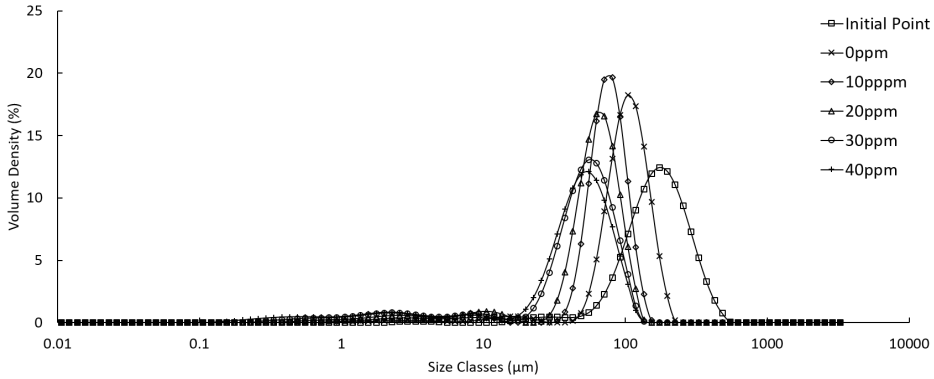

Figure 5.3: Emulsion droplet size distribution of silicone oil 50 in 3.5wt% NaCl brine with SDBS surfactant (0, 10, 20, 30, 40ppm)

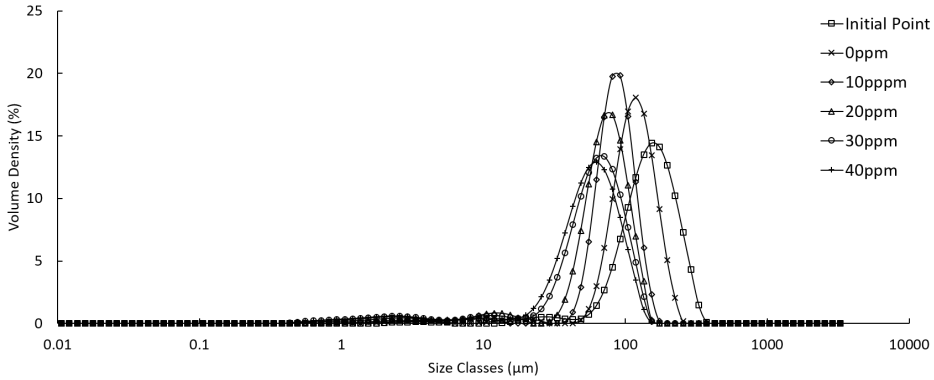

Figure 5.4: Emulsion droplet size distribution of silicone oil 100 in 3.5wt% NaCl brine with SDBS surfactant (0, 10, 20, 30, 40ppm)

Above Figure 5.3 and Figure 5.4 represent the silicone oil 50 and silicone oil 100 droplet size distribution in 3.5wt% NaCl brine with various SDBS surfactant concentra-

tion.

It is fairly hard to find any difference between silicone oil 50 and silicone oil 100 droplet size distribution. The pattern that emulsion droplet size distribution looks very similar. However, the sharpness of the curve is somewhat different. The width of the curve in Figure 5.3 is wider than the curve in Figure 5.4. This indicates that the polydispersity of emulsion droplet size is relatively higher with low viscosity dispersed phase.

The viscosity also affects to the maximum droplet size within the emulsion. As shown in Table 5.5, the overall dv95 values with the silicone oil 100 are higher than the dv95 values with the silicone oil 50.

Concentration (ppm)	dv95 with silicone oil 50 (μm)	dv95 with silicone oil 100 (μm)
0ppm	169	189
10ppm	117	133
20ppm	104	121
30ppm	96.6	115
40ppm	93.8	107

Table 5.5: dv95 value comparison between silicone oil 50 and silicone oil 100 with different surfactant concentration

5.2.2 Different types of surfactants

In this experiment, three different kinds of surfactants are utilized to investigate their influence on the emulsion droplet size distribution. These are sodium dodecylbenzene sulfonate (SDBS), sodium *bis*(2-ethylhexyl) sulfosuccinate (AOT) and Span® 80. Both SDBS and AOT are the anionic surfactant, but different molecular structure. On the other hand, Span® 80 is a non-ionic surfactant which can be soluble in silicone oil.

To investigate their influence on the droplet size distribution, all other variables are controlled except for the type of surfactants and Span® 80 surfactant concentration. However, the range of interfacial tension with Span® 80 is relatively similar to those interfacial tensions with SDBS and AOT. Therefore, it is reasonable to compare these result regardless of the Span® 80 concentration. The results are shown in Figure 5.5, 5.6 and 5.7.

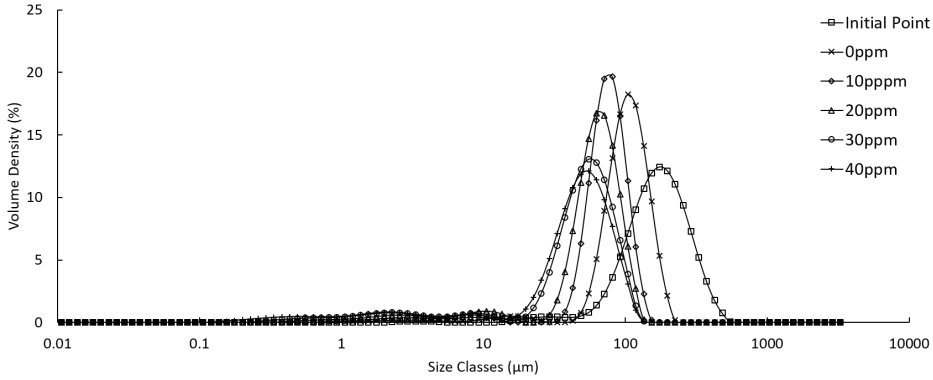

Figure 5.5: Emulsion droplet size distribution of silicone oil 50 in 3.5wt% NaCl brine with SDBS surfactant (0, 10, 20, 30, 40ppm)

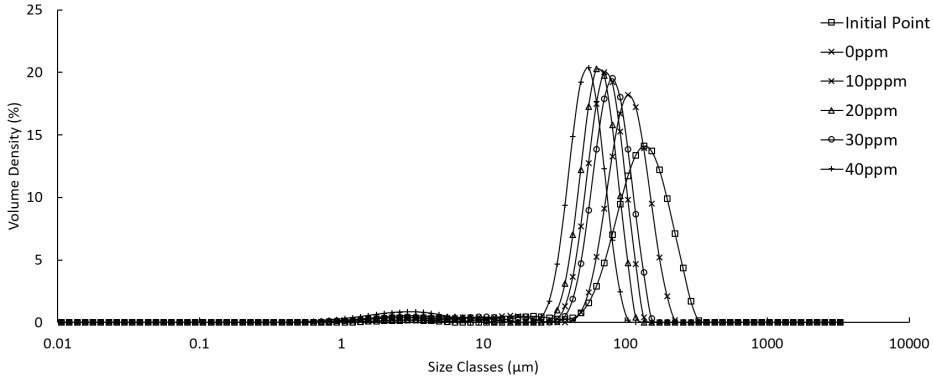

Figure 5.6: Emulsion droplet size distribution of silicone oil 50 in 3.5wt% NaCl brine with AOT surfactant (0, 10, 20, 30, 40ppm)

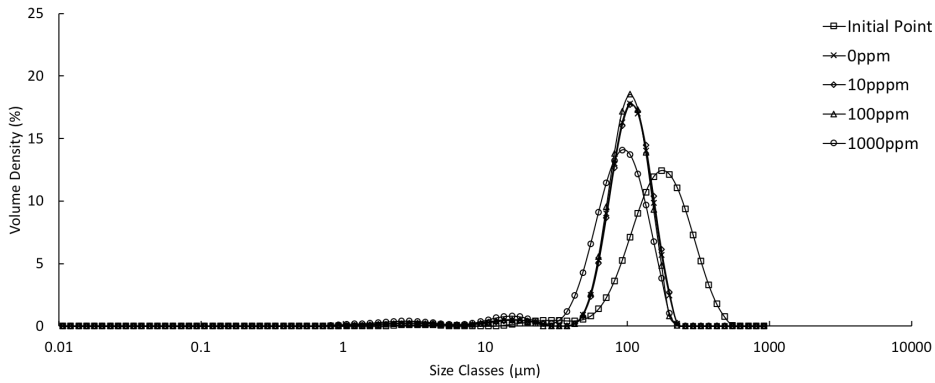

Figure 5.7: Emulsion droplet size distribution of silicone oil 50 in 3.5wt% NaCl brine with Span® 80 surfactant (0, 10, 100, 1000ppm)

The major observation from the result is the evolution pattern of droplet size distribution. The droplet size distribution of all three cases shows similar trend until 10ppm of surfactant concentration. However, the polydispersity of droplet size with SDBS dramatically increases whereas the emulsion with AOT shows decreasing polydispersity trend and gets more sharpening its droplet size distribution. On the other hand, emulsion with span® 80 maintains its droplet size distribution for a while, but ultimately its polydispersity increases producing smaller droplets.

From the Figure 5.5 and 5.7, the emulsion droplet size distribution can be divided into following two stages. The first stage shows a pattern that the shape of the droplet size distribution curve gets sharpened and the median point moves to the left side at the same time. This means the breakage of the emulsion droplets while the polydispersity is decreasing. In this case, this happens from the initial point to the surfactant concentration of 10ppm. The second stage shows a pattern that the shape of the droplet size distribution curve gets wider while the median point still moves to the left-hand side. This indicates that the smaller size of the emulsion droplets is produced by continuous mixing energy input. During the first step, large size emulsion droplets are being broken while medium-size emulsion droplets are being broken during the second stage.

Different from the Figure 5.5 and 5.7, Figure 5.6 does not show the above illustrated second stage. This means that mainly larger size emulsion droplets are being broken up while the population of smaller size droplets is maintained. The major difference is that AOT has double tailed structure while SDBS and span® 80 has single tailed structure. Therefore, this demonstrates that the structure of the surfactant can significantly influence on the emulsion droplet size distribution.

5.2.3 Salinity of continuous phase

The influence of the continuous phase salinity on the emulsion droplet size distribution was also investigated in this experiment. To examine this effect, four different kinds of continuous phase were used. Figure 5.8, 5.9, 5.10 and 5.11 illustrate the emulsion droplet size distribution of silicone oil 50 with SDBS surfactant in MQ water, 0.1wt% NaCl brine, 3.5wt% NaCl brine and 25wt% NaCl brine respectively. MQ water represents deionized water and the amount of sodium ion and chloride ion in the continuous phase increases as the NaCl concentration increases.

According to the distribution pattern, Figure 5.8 and 5.9 can be grouped together and Figure 5.10 and 5.11 can be lumped together. These groups show a distinct difference between low salinity and high salinity.

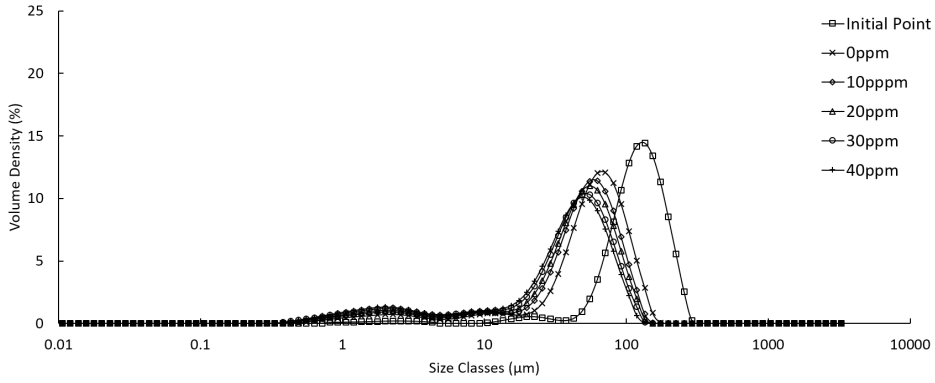

Figure 5.8: Emulsion droplet size distribution of silicone oil 50 in deionized water(MQ water) with SDBS surfactant (0, 10, 20, 30, 40ppm)

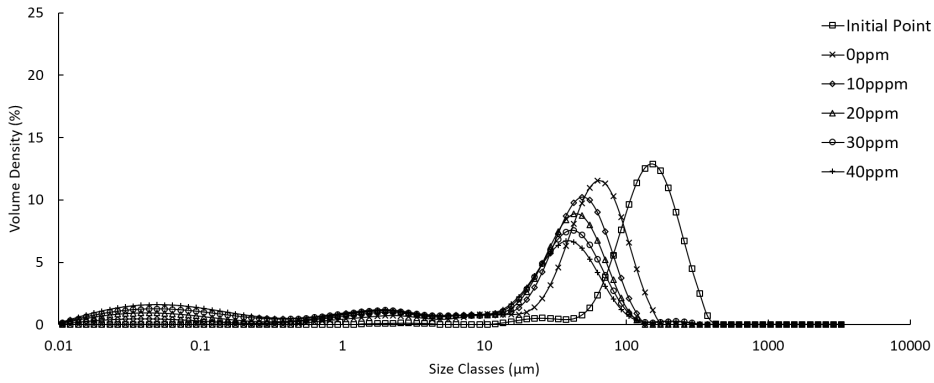

Figure 5.9: Emulsion droplet size distribution of silicone oil 50 in 0.1wt% NaCl brine with SDBS surfactant (0, 10, 20, 30, 40ppm)

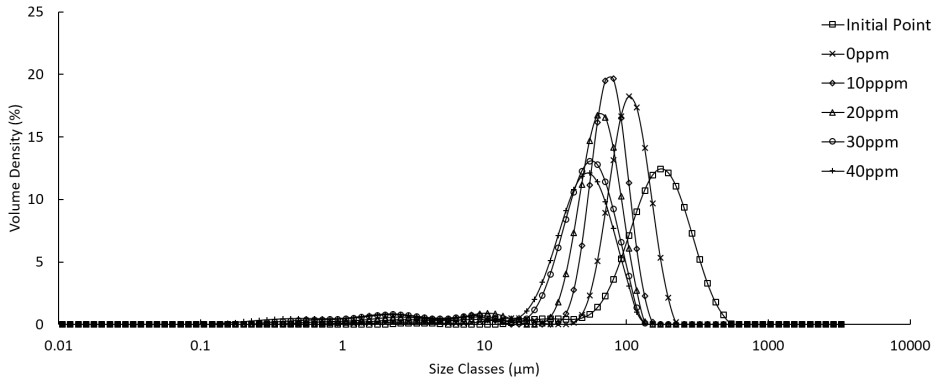

Figure 5.10: Emulsion droplet size distribution of silicone oil 50 in 3.5wt% NaCl brine with SDBS surfactant (0, 10, 20, 30, 40ppm)

Polydispersity is also a major difference between the two groups. The polydispersity was kept increasing as surfactant concentration increases when both MQ water and 0.1wt% NaCl solution were continuous phases. Meanwhile, the polydispersity of Figure 5.10 and Figure 5.11 decreases at first and starts to increase after surfactant concentration of 20ppm. This can be explained related to the emulsion stability.

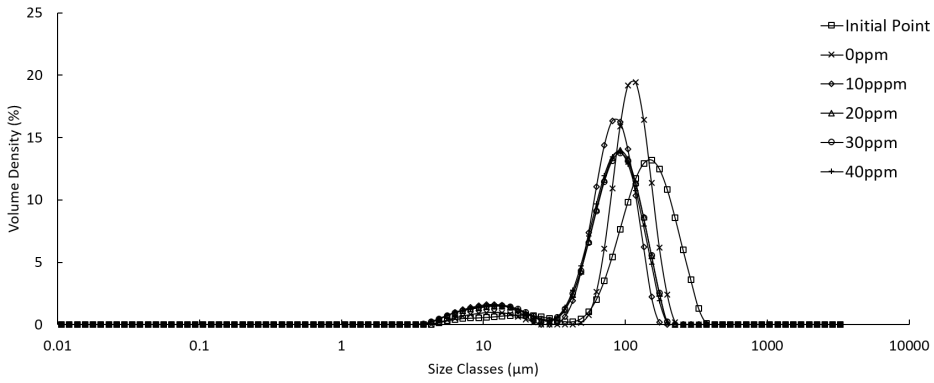

Figure 5.11: Emulsion droplet size distribution of silicone oil 50 in 25wt% NaCl brine with SDBS surfactant (0, 10, 20, 30, 40ppm)

5.2.4 Dispersed phase volume fraction

The effect of dispersed phase volume fraction on the droplet size distribution was also investigated by changing the amount of silicone oil within the emulsion. Below Figure 5.12, 5.13 and 5.14 represent droplet size distribution of silicone oil 50 in 3.5wt% NaCl brine with dispersed volume fraction 0.1%, 0.5% and 1%(v/v).

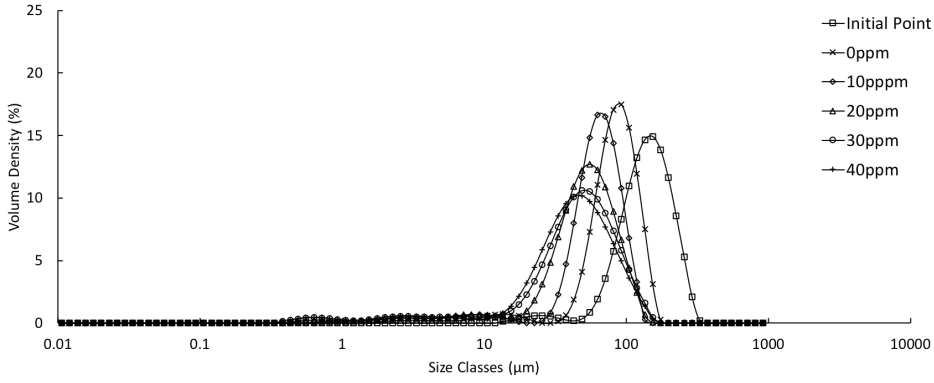

Figure 5.12: Emulsion droplet size distribution of silicone oil 50 in 3.5wt% NaCl brine with SDBS surfactant (0, 10, 20, 30, 40ppm), Dispersed phase volume fraction = 0.1%(v/v)

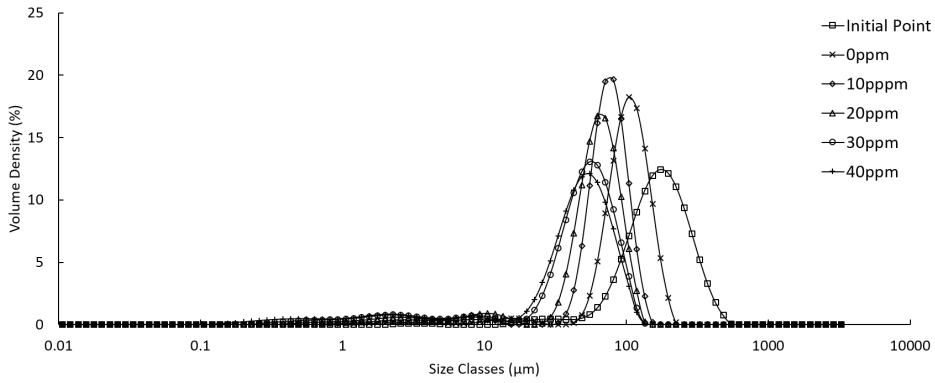

Figure 5.13: Emulsion droplet size distribution of silicone oil 50 in 3.5wt% NaCl brine with SDBS surfactant (0, 10, 20, 30, 40ppm), Dispersed phase volume fraction = 0.5%(v/v)

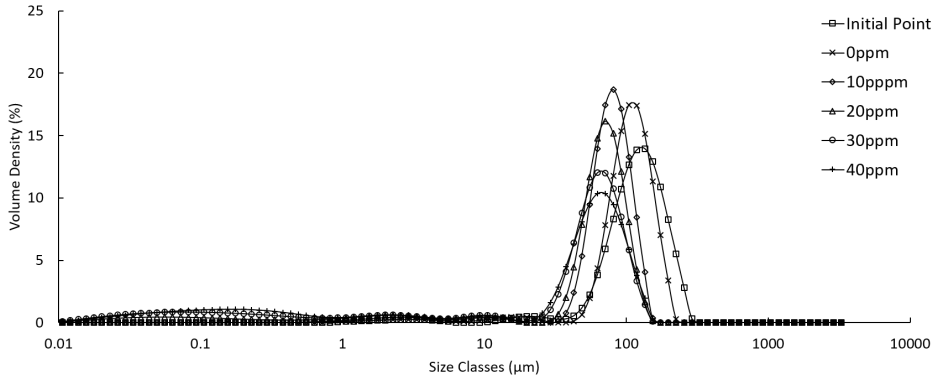

Figure 5.14: Emulsion droplet size distribution of silicone oil 50 in 3.5wt% NaCl brine with SDBS surfactant (0, 10, 20, 30, 40ppm), Dispersed phase volume fraction = 1%(v/v)

Based on the observation, the evolution of droplet size distribution and its pattern showed a very similar trend. At the same time, the sizes of the droplet in all three cases were also comparable to each other. However, the polydispersity of emulsion tends to decrease with increasing dispersed phase volume fraction.

5.3 Droplet size prediction

For the prediction of maximum droplet size, dv95 values from eight experimental cases in Table 5.6 were used. Each cases contain dv95 values with six different surfactant concentration, which are 0, 10, 20, 30, 40 and 50ppm except for the case 4 and 6. In case 4, it contains dv95 values with surfactant concentration of 0, 10, 100 and 1000ppm and in case 6, dv95 values with surfactant concentration of 0, 10, 20, 30 40ppm are involved.

Case no.	Type of silicone oil	Type of surfactant	Continuous phase	Dispersed phase volume fraction (v/v)
1	Silicone oil 50	SDBS	3.5wt% NaCl brine	0.5%
2	Silicone oil 100	SDBS	3.5wt% NaCl brine	0.5%
3	Silicone oil 50	AOT	3.5wt% NaCl brine	0.5%
4	Silicone oil 50	Span® 80*	3.5wt% NaCl brine	0.5%
5	Silicone oil 50	SDBS	MQ water	0.5%
6	Silicone oil 50	SDBS	0.1wt% NaCl brine	0.5%
7	Silicone oil 50	SDBS	3.5wt% NaCl brine	0.1%
8	Silicone oil 50	SDBS	3.5wt% NaCl brine	1%

Table 5.6: List of the experiments conducted with surfactant concentration of 10, 20, 30, 40 ppm
*Only Span® 80 concentration is different with other surfactant (10, 100, 1000ppm)

5.3.1 Calculation of maximum drop diameter

To be able to predict the maximum size of the droplet in emulsion accurately, numerical coefficients in Equation 3.8, 3.9, and 3.10 need to be adequately determined. To calculate these numerical coefficients, maximum droplet size needs to be obtained experimentally. Since dv95 value has been regarded as a maximum drop size from previous studies[5, 7, 40, 42, 53], dv95 values from the experiment was used to calculate the numerical coefficients.

For about the Equation 3.8, there are two ways to estimate the numerical coefficient A_1. Since the numerical coefficient A_1 is the only unknown value in Equation 3.8, it can be easily calculated by substituting corresponding values like average energy dissipation rate, interfacial tension and mass density of continuous phase.

But, there are two ways to calculate the numerical coefficient A_1. One way of calculation is to use the principle of least squares by minimizing the sum of squared residuals. Another way of A_1 estimation is to use linear relationship since terms in the left-hand side and right-hand side of Equation 3.8 are in a linear relationship. In this paper, the principle of least squares was used for convenience because these two methods provide an identical solution after all.

The principle of least squares was also used to calculate coefficients in Equation 3.9 and 3.10. Experimentally obtained dv95 was substituted in D_{max} on the right hand side of Equation 3.9 and 3.10. Viscosity and mass density of dispersed phase was also used for the better model fitting. Alike Equation 3.8, numerical coefficients, A_2, A_3 and A_4, A_5, were determined toward minimizing sum of squared residuals.

5.3.2 Numerical coefficient

Following Table 5.7 representsthe calculated numerical coefficient of Equation 3.8, 3.9 and 3.10 for each cases in Table 5.6.

Case no.	A1	A2	A3	A4	A5
1	0.132	0.080	0.068	0.080	0.066
2	0.150	0.090	0.033	0.090	0.032
3	0.131	0.090	0.047	0.090	0.046
4	0.140	0.030	0.860	0.030	0.829
5	0.071	0.072	0	0.072	0
6	0.074	0.074	0.002	0.074	0
7	0.120	0.060	0.130	0.060	0.126
8	0.142	0.090	0.064	0.090	0.062

Table 5.7: Numerical coefficient for Equation 3.8, 3.9 and 3.10 for each cases

Below Table 5.8 shows the numerical coefficient from previous studies depending on the homogenizer type. Compare to early studies, numerical coefficient from the current study is much smaller. It is more obvious when it comes to the coefficient A_3 and A_5. Also, each system has its own numerical coefficient, so that it cannot be represented by unique value.

5.3.3 Correlation between experimental and theoretical value

In this section, the correlations between the dv95 value obtained by experiment and the theoretically estimated maximum droplet size are presented for all eight cases in Table 5.6. In each case, dv95 values with different concentration are compared to D_KH, D_D, and D_C values respectively. D_KH means the maximum droplet diameter calculated by Kolmogorov-Hinze theory (Equation 3.8). D_D means the maximum droplet diameter

Study	Homogenizer type	A_2 or A_4	A_3 or A_5
Davies[10]	-	≈1.0	≈0.35
Sprow[42]	Impellers	0.138	Not defined
Calabrese et al.[6, 54]	Impellers	≈0.09	≈3.5
Berkman and Calabrese[4]	Static mixer	0.416	1.47
Hinze[21]	Coaxial cylinders	0.725	Not defined
Vankova et al.[47]	Narrow-gap homogenizer	0.86	0.37

Table 5.8: Values of numerical coefficient in previous studies with corresponding homogenizer type

calculated by Equation 3.9. And D_C means the maximum droplet diameter calculated by Equation 3.10. In each plot, the y-axis indicates the experimental dv95 value and the x-axis indicates D_KH, D_D, and D_C. The diagonal dash line is $y = x$ line, which is an equivalent line.

As seen in blow figures, D_D and D_C show much better in accordance with the model than D_KH, which is Kolmogorov-Hinze theory. This is because D_D and D_C contain dispersed viscosity term within the equations(Equation 3.9 and 3.10). On the other hand, very little difference was observed between D_D and D_C. This is because the difference in mass density of the continuous phase and dispersed phase is very low. Therefore, Equation 3.9 is sufficient to approximate the result in this experiment.

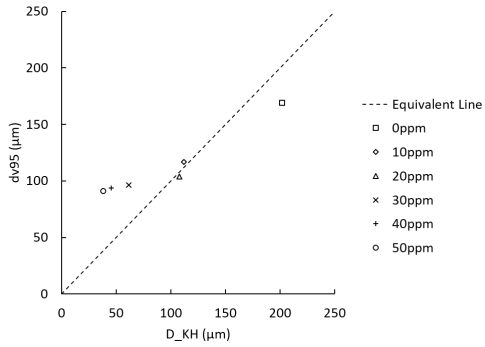

Figure 5.15: Case 1: Correlation between experimental results (dv95) and theoretically predicted values (D_KH)

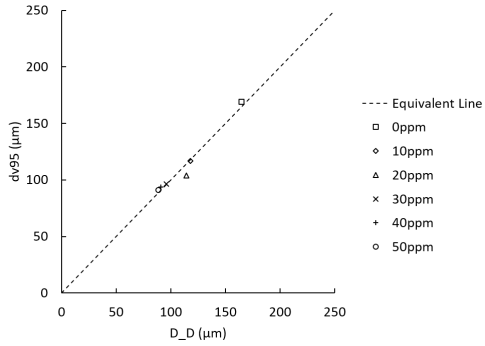

Figure 5.16: Case 1: Correlation between experimental results (dv95) and theoretical prediction (D_D)

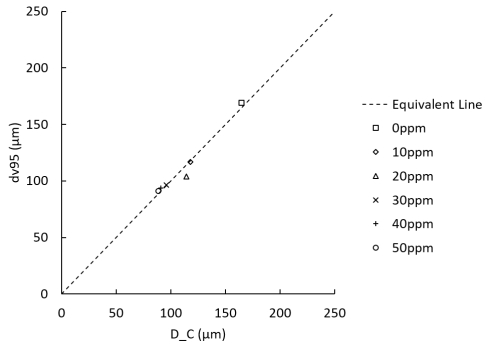

Figure 5.17: Case 1: Correlation between experimental results (dv95) and theoretical prediction (D_C)

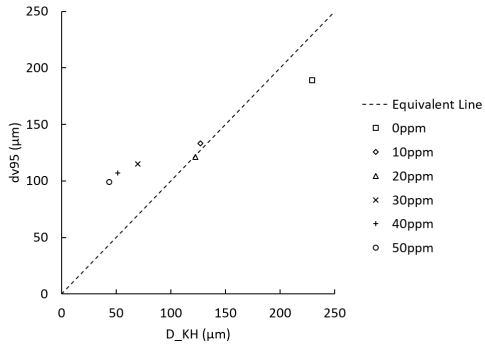

Figure 5.18: Case 2: Correlation between experimental results (dv95) and theoretically predicted values (D_KH)

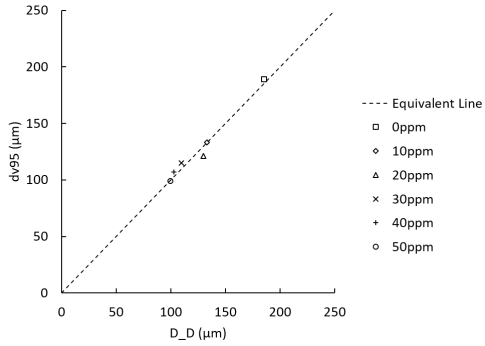

Figure 5.19: Case 2: Correlation between experimental results (dv95) and theoretical prediction (D_D)

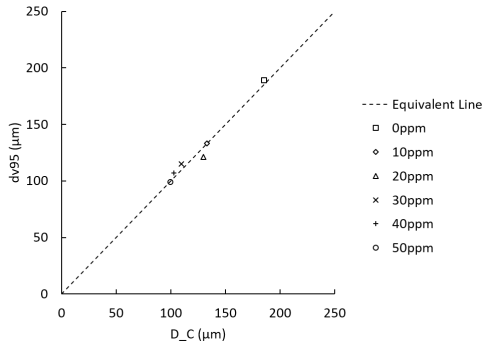

Figure 5.20: Case 2: Correlation between experimental results (dv95) and theoretical prediction (D_C)

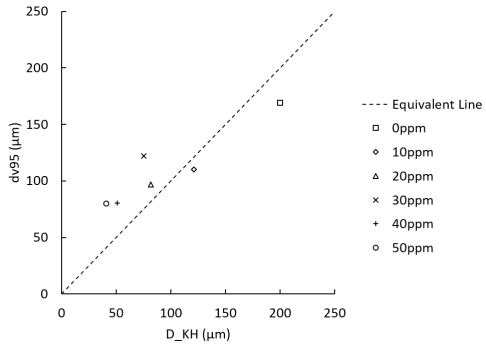

Figure 5.21: Case 3: Correlation between experimental results (dv95) and theoretically predicted values (D_KH)

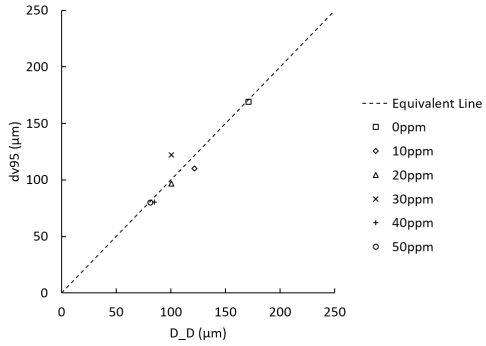

Figure 5.22: Case 3: Correlation between experimental results (dv95) and theoretical prediction (D_D)

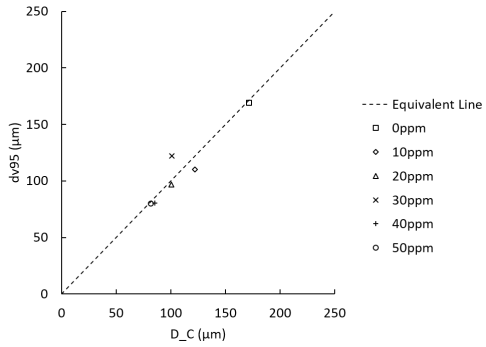

Figure 5.23: Case 3: Correlation between experimental results (dv95) and theoretical prediction (D_C)

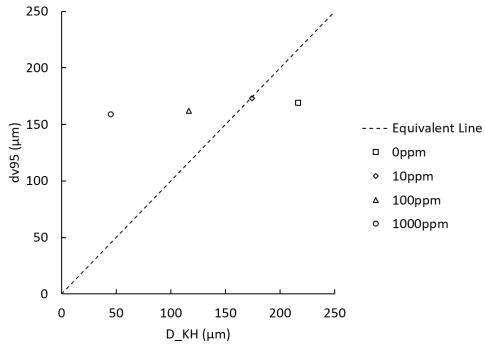

Figure 5.24: Case 4: Correlation between experimental results (dv95) and theoretically predicted values (D_KH)

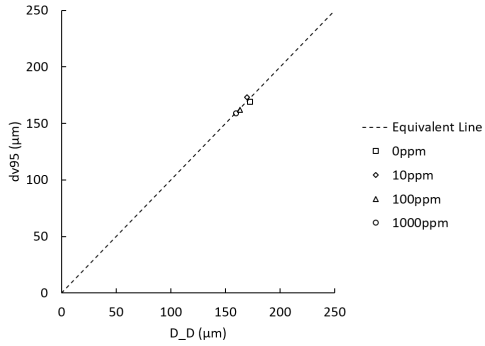

Figure 5.25: Case 4: Correlation between experimental results (dv95) and theoretical prediction (D_D)

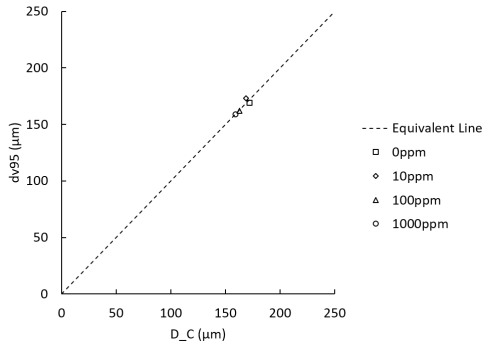

Figure 5.26: Case 4: Correlation between experimental results (dv95) and theoretical prediction (D_C)

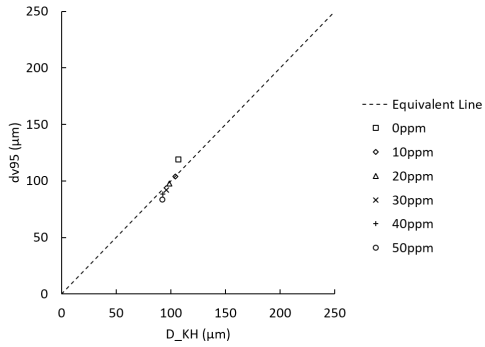

Figure 5.27: Case 5: Correlation between experimental results (dv95) and theoretically predicted values (D_KH)

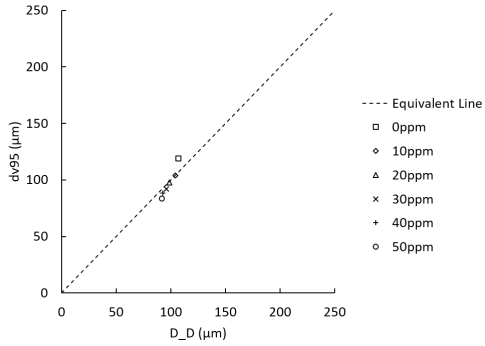

Figure 5.28: Case 5: Correlation between experimental results (dv95) and theoretical prediction (D_D)

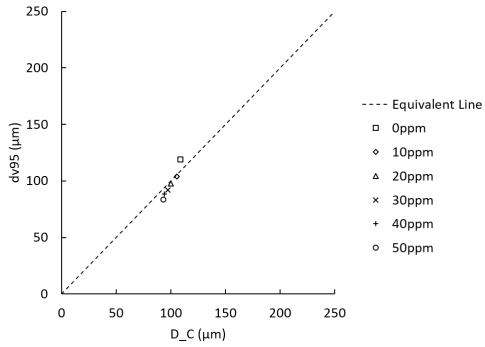

Figure 5.29: Case 5: Correlation between experimental results (dv95) and theoretical prediction (D_C)

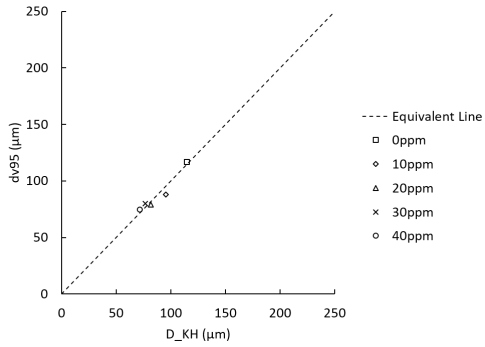

Figure 5.30: Case 6: Correlation between experimental results (dv95) and theoretically predicted values (D_KH)

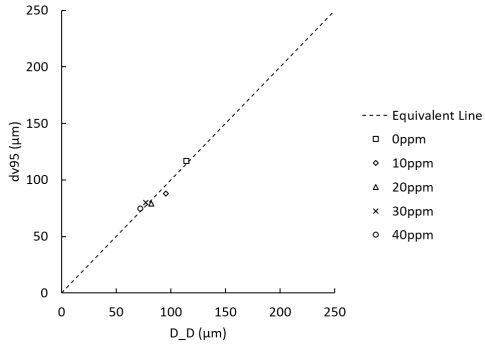

Figure 5.31: Case 6: Correlation between experimental results (dv95) and theoretical prediction (D_D)

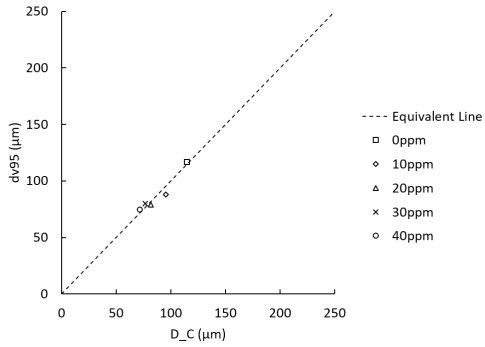

Figure 5.32: Case 6: Correlation between experimental results (dv95) and theoretical prediction (D_C)

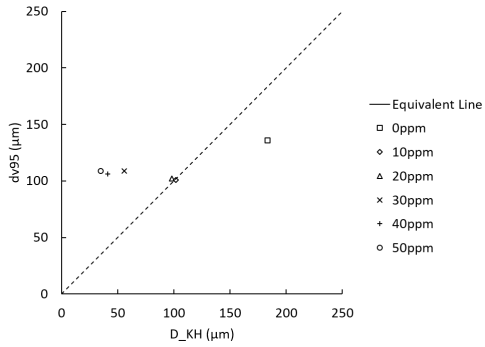

Figure 5.33: Case 7: Correlation between experimental results (dv95) and theoretically predicted values (D_KH)

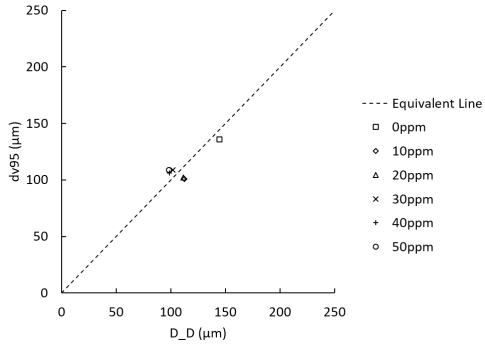

Figure 5.34: Case 7: Correlation between experimental results (dv95) and theoretical prediction (D_D)

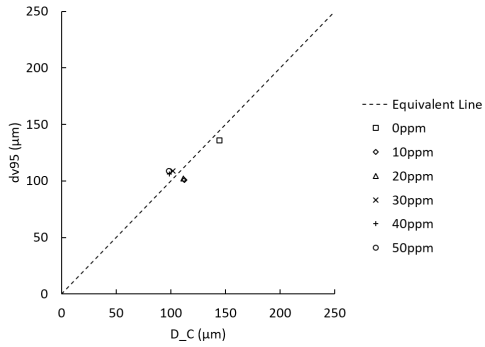

Figure 5.35: Case 7: Correlation between experimental results (dv95) and theoretical prediction (D_C)

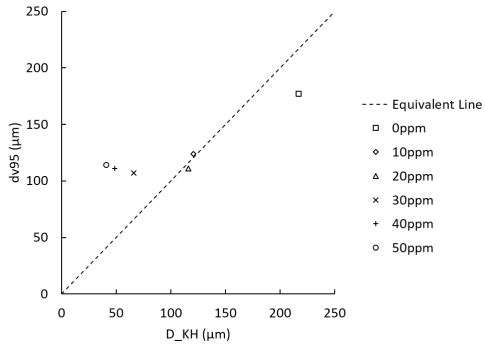

Figure 5.36: Case 8: Correlation between experimental results (dv95) and theoretically predicted values (D_KH)

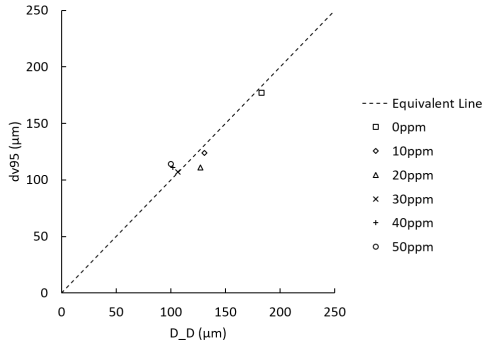

Figure 5.37: Case 8: Correlation between experimental results (dv95) and theoretical prediction (D_D)

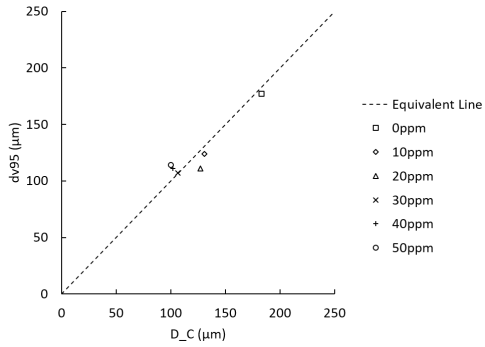

Figure 5.38: Case 8: Correlation between experimental results (dv95) and theoretical prediction (D_C)

Chapter 6

Discussion

6.1 Influence on the droplet size distribution

From the emulsion droplet size distribution, the shape of the droplet size distribution curve and the evolution of the curve according to the surfactant concentration are the main matters that can be observed. Based on this information, the polydispersity of emulsion can be estimated qualitatively as well. So, in this chapter, these will be primarily discussed based on the variables such as dispersed phase viscosity, type of surfactant, the salinity of continuous phase and the dispersed phase volume fraction.

6.1.1 Influence of viscosity

The viscosity of dispersed phase influences on the overall shape of the emulsion droplet size distribution curve, but not on the evolution of droplet size distribution. This is essentially related to the polydispersity of the emulsion. The higher viscosity of dispersed phase leads to lower polydispersity whereas the lower viscosity of the dispersed phase causes higher polydispersity of emulsion as shown in Figure 5.3 and 5.4.

The viscosity of the dispersed phase also affects on the overall size of the droplet in the

emulsion. As seen in Table 5.5, the dv95 values with dispersed phase with higher viscosity are higher than the dv95 values with dispersed phase with low viscosity under the same level of energy input. The viscosity difference between silicone oil 50 and 100 is 47.95 $mPa \cdot s$ and this induces emulsion droplet size difference of approximately 20μm in every surfactant concentration.

Therefore, it is reasonable to conclude that the viscosity of dispersed phase effects on the overall shape of the emulsion droplet size distribution and its polydispersity. Also, the higher viscosity of dispersed phase yields the larger size of emulsion droplet, because oil droplet with higher viscosity requires more energy to break up than oil droplet with less viscosity.

6.1.2 Influence of surfactant type

In this experiment, three different types of surfactants such as sodium dodecylbenzene sulfonate (SDBS), sodium *bis*(2-ethylhexyl) sulfosuccinate (AOT) and Span® 80 were used and the emulsion droplet size distribution of each cases are depicted in Figure 5.5, 5.6 and 5.7. The type of surfactant primarily influence on the evolution and shape of droplet size distribution curve, polydispersity and also on the emulsion droplet size.

First, Figure 5.5 and 5.6 shows the droplet size distribution of emulsion with SDBS, AOT. Both surfactants are the anionic surfactant and the experiment was conducted in the same condition. This means that the discrepancy in the results is caused by the chemical structure of the surfactant in nature. AOT has a double tail in terms of its chemical structure whereas SDBS has a single tail with the benzene ring in its chemical structure. Because of its chemical structure, AOT tends to form microemulsions when it adsorbs at oil-water interface without co-solvent or co-surfactant. On the other hand, SDBS is not capable to produce microemulsions without co-surfactant. This means that once these surfactants are adsorbed at the interface between oil in water, AOT gives more stability than SDBS. Therefore, as seen in Figure 5.6, the smaller droplets do not readily break-up maintaining

its population and ultimately decrease the emulsion polydispersity. This is the reason why the polydispersity increases at relatively high surfactant concentration.

Compared to SDBS and AOT, Span® 80 is a non-ionic surfactant and does not react with ionic ingredients and electrolyte. Therefore, the stability of emulsion with Span® 80 is very high as shown in Figure 5.7. However, the overall droplet size of the emulsion decreases as the surfactant concentration increases for all three types of surfactants.

To summarize, different types of surfactants influence on the evolution and shape of the emulsion droplet size distribution curve and this is primarily related to the stability and polydispersity of the emulsion. Also, an increase in surfactant concentration causes a decrease in overall droplet size in the emulsion.

6.1.3 Influence of continuous phase salinity

The influence of continuous phase salinity was investigated by changing the concentration of NaCl. Figure 5.8, 5.9, 5.10 and 5.11 proved that the salinity of continuous phase plays major role in terms of emulsion stability and polydispersity.

This can be explained by the interrelationship between ionic surfactant and electrolyte. When there is an oil droplet covered by ionic surfactant in the electrolyte, ions in the electrolyte are attracted toward the oil droplet and consequently, the ionic concentration nearby the oil droplet increases. This results in the formation of the electrical double layer on the oil droplet surface. When the concentration of the electrolyte is high, diffuse layer extension of the electrical double layer decreases causing lower zeta potential. The stability of the emulsion is low at lower zeta potential.

Another factor that needs to be considered is packing of surfactants at the interface. At high concentration of the electrolyte, the packing of surfactant at the interface increases. Therefore, increased salinity of continuous phase gives higher surfactant packing increasing emulsion stability.

In above cases, it is obvious to say that 3.5wt% NaCl solution and 20wt% NaCl so-

lution contains much more ions compared to the MQ water and 0.1wt% NaCl solution. Then more ions are prone to be attractive and form the electrical double layer. This results in low zeta potential and low emulsion stability. On the other hand, the surfactant packing increases with increasing electrolyte concentration, which gives higher emulsion stability. So, emulsion with 3.5wt% NaCl solution and 20wt% solution as continuous phase has higher emulsion stability than emulsion with MQ water and 0.1wt% NaCl solution as a continuous phase, giving low polydispersity. Therefore, 20ppm, 30ppm and 40ppm curves in Figure 5.11 stay in the same position due to the extremely high emulsion stability.

Therefore, it can be concluded that higher salinity of continuous phase yields higher stability of the emulsion and lower emulsion polydispersity because of the higher surfactant packing.

6.1.4 Influence of dispersed phase volume fraction

Change in volume fraction will affect the density of the liquid in the tank as well as collision frequency of droplets in turbulent. The more dispersed phase volume fraction, the more collision will occur.

When the collision rate is high, droplet coalescence is more likely to occur. However, from the current droplet size distribution data, polydispersity is the only thing that can be observed. It shows that polydispersity decreases as the dispersed phase volume fraction increases. But still, it is hard to infer the relationship between droplet coalescence and the polydispersity from the current droplet size distribution data.

6.2 Model accordance

The numerical coefficients of Equation 3.8, 3.9, and 3.10 were determined by using the least square method and the maximum size of the droplet in the emulsion for the eight

cases in Table 5.6 was predicted. The numerical coefficients of each case are listed in Table 5.7.

According to the result, each system has its own numerical coefficient. In other words, there is no single value that can be utilized for all systems. However, these numerical coefficient represent the characteristics of each system and obviously, there exist some trend that can be deduced from the result. This is shown in Table 6.1.

Variable change	Case no.	Change in A_1, A_2 and A_4	Change in A_3 and A_5
Increase in dispersed phase viscosity	1, 2	Increase	Decrease
Increase in continuous phase salinity	5, 6, 1	Increase	Increase
Increase in dispersed phase volume fraction	1, 3, 4	Increase	Decrease

Table 6.1: Change in numerical coefficient depending on the variables

To compare this numerical coefficient with other studies, in Table 5.8, values calculated in this thesis are generally smaller than previously estimated values from others. This can be interpreted that the numerical coefficient varies depending on the experimental technique and materials used in the experiment. This also supports the statement that each system has its own unique numerical coefficient.

Therefore, it is essential to know about the system thoroughly, so that it can be well characterized and gives better predictions of the maximum size of the droplet in the given emulsion.

Chapter 7

Conclusion

In this project, the breakage of the oil-in-water emulsion droplet was investigated experimentally. The experiments were conducted by using a laser diffraction method and spinning drop method for measuring droplet size distribution and interfacial tension.

As a dispersed phase, silicone oils with two different viscosity were used. For the continuous phase, MQ water, 0.1wt%, 3.5wt% with three different kinds of surfactant were utilized. The surfactant concentration was also varied to investigate its influence.

The oil-in-water emulsion droplet size distribution under different conditions was analyzed in terms of the dispersed phase viscosity, types of surfactant, the salinity of the continuous phase and the dispersed phase volume fraction. Mainly, the evolution and shape of the droplet size distribution curve in accordance with the surfactant concentration were investigated. The polydispersity of emulsion droplet size was also analyzed qualitatively.

At first, the viscosity of dispersed phase effects to both the overall shape of the emulsion droplet size distribution and its polydispersity. It showed that the higher viscosity of dispersed phase gives the larger size of the emulsion droplet.

Secondly, the different types of surfactants have an impact on the evolution and shape of the emulsion droplet size distribution curve and it is primarily related to the emul-

sion stability and the polydispersity. Additionally, an increase in surfactant concentration causes a decrease in overall emulsion droplet size.

In case of the salinity of the continuous phase, the higher continuous phase salinity yields the higher stability of the emulsion. Also, it decreases the polydispersity of emulsion droplet size because of the higher surfactant packing on the interface.

Finally, the influence of the dispersed phase volume fraction was investigated and the result showed that polydispersity decreases as the dispersed phase volume fraction increases. However, it is difficult to find the relationship between droplet size distribution and dispersed phase volume fraction in the emulsion.

Based on the experimental result, the maximum size of the droplet was predicted using Kolmogorov-Hinze theory. Further developed models which account for the dispersed phase viscosity and mass density difference between two phases were also utilized for maximum droplet size prediction.

The numerical coefficients in each model were determined by using the least square method. It was concluded that each system has its own numerical coefficient and there is no single value that can be utilized for all systems. Therefore, it is necessary to know about the system thoroughly for better prediction of maximum droplet size in the emulsion.

Bibliography

[1] G. Batchelor. Pressure fluctuations in isotropic turbulence. In *Mathematical Proceedings of the Cambridge Philosophical Society*, volume 47, pages 359–374. Cambridge University Press, 1951.

[2] G. K. Batchelor. *The theory of homogeneous turbulence*. Cambridge university press, 1953.

[3] B. Bedwell and E. Gulari. Electrolyte-moderated interactions in water/oil microemulsions. *Journal of colloid and interface science*, 102(1):88–100, 1984.

[4] P. D. Berkam and R. V. Calabrese. Dispersion of viscous fluids by turbulent flow in a static mixer. *AIChE Journal*, 34(4):602–609, 1988.

[5] S. M. Bhavaraju, T. W. Russell, and H. W. Blanch. The design of gas sparged devices for viscous liquid systems. *AIChE Journal*, 24(3):454–466, 1978.

[6] R. V. Calabrese, T. P. K. Chang, and P. T. Dang. Drop breakup in turbulent stirred tank contactors. Part I: Effect of dispersed phase viscosity. *AIChE Journal*, 32(4):657–666, 1986.

[7] H. T. Chen and S. Middleman. Drop Size Distribution in Agitated Liquid-Liq uid Systems. *AIChE J.*, 13(5):989–995, 1967.

[8] O. Commission et al. Discharges, spills and emissions from offshore oil and gas installations in 2009, including assessment of data reported in 2008 and 2009, 2012.

[9] C. A. Coulaloglou and L. L. Tavlarides. Description of interaction processes in agitated liquid-liquid dispersions. *Chemical Engineering Science*, 32(11):1289–1297, 1977.

[10] J. T. Davies. Drop sizes of emulsions related to turbulent energy dissipation rates. *Chemical Engineering Science*, 40(5):839–842, 1985.

[11] W. F. Directive. A framework for community action in the field of water policy. 2000.

[12] J. Drelich, C. Fang, and C. White. Measurement of interfacial tension in fluid-fluid systems. *Encyclopedia of surface and colloid science*, 3:3158–3163, 2002.

[13] A. Fakhru'l-Razi, A. Pendashteh, L. C. Abdullah, D. R. A. Biak, S. S. Madaeni, and Z. Z. Abidin. Review of technologies for oil and gas produced water treatment. *Journal of Hazardous Materials*, 170(2-3):530–551, 2009.

[14] L.-G. Faksness, P. G. Grini, and P. S. Daling. Partitioning of semi-soluble organic compounds between the water phase and oil droplets in produced water. *Marine pollution bulletin*, 48(7):731–742, 2004.

[15] K. Fontell. The structure of the lamellar liquid crystalline phase in aerosol otwater system. *Journal of Colloid and Interface Science*, 44(2):318–329, 1973.

[16] A. Grant and A. D. Briggs. Toxicity of sediments from around a North Sea oil platform: Are metals or hydrocarbons responsible for ecological impacts? *Marine Environmental Research*, 53(1):95–116, 2002.

[17] O. Hanssens. *Petroleum on the Norwegian Continental Shelf 2014 Fields and Discoveries*. 2014.

[18] M. Hasegawa, Y. Yamasaki, N. Sonta, Y. Shindo, T. Sugimura, and A. Kitahara. Clustering of aerosol ot reversed micelles as studied by nonradiative energy transfer of solubilized probes. *The Journal of Physical Chemistry*, 100(38):15575–15580, 1996.

[19] L. M. He, L. L. Kear-Padilla, S. H. Lieberman, and J. M. Andrews. Rapid in situ determination of total oil concentration in water using ultraviolet fluorescence and light scattering coupled with artificial neural networks. *Analytica Chimica Acta*, 478(2):245–258, 2003.

[20] M. S. Hellsing, A. R. Rennie, and A. V. Hughes. Effect of concentration and addition of ions on the adsorption of aerosol-ot to sapphire. *Langmuir*, 26(18):14567–14573, 2010.

[21] J. O. Hinze. Fundamentals of the hydrodynamics mechanisms of splitting in dispersion process. *AIChE Journal*, 1(3):289–295, 1955.

[22] HORIBA scientific. Understanding and interpreting particle size distribution calculations, 2018.

[23] E. T. Igunnu and G. Z. Chen. Produced water treatment technologies. *International Journal of Low-Carbon Technologies*, 9(3):157–177, 2012.

[24] H. A. Jakobsen. *Chemical reactor modeling: multiphase reactive flows*. Springer Science & Business Media, 2014.

[25] S. Johnsen, T. I. Røe Utvik, E. Garland, B. de Vals, J. Campbell, et al. Environmental fate and effect of contaminants in produced water. In *SPE International Conference on Health, Safety, and Environment in Oil and Gas Exploration and Production*. Society of Petroleum Engineers, 2004.

[26] A. Kolmogorov. On the breakage of drops in a turbulent flow. In *Dokl. Akad. Navk. SSSR*, volume 66, pages 825–828, 1949.

[27] R. Kuboi, I. Komasawa, and T. Otake. Collision and coalescence of dispersed drops in turbulent liquid flow. *Journal of Chemical Engineering of Japan*, 5(4):423–424, 1972.

[28] J. Lagisetty, P. Das, R. Kumar, and K. Gandhi. Breakage of viscous and non-newtonian drops in stirred dispersions. *Chemical Engineering Science*, 41(1):65–72, 1986.

[29] K. Lee and J. Neff. *Produced Water - Environmental risks and advances in mitigation technologies.* Number 1. 2011.

[30] D. Li, editor. *Weber Number*, pages 2185–2185. Springer US, Boston, MA, 2008.

[31] H. Lindner, G. Fritz, and O. Glatter. Measurements on Concentrated Oil in Water Emulsions Using Static Light Scattering. *Journal of Colloid and Interface Science*, 242(1):239–246, 2001.

[32] Malvern Instruments Ltd. Mie theory The first 100 years. 2010.

[33] C. Manning and L. Scriven. On interfacial tension measurement with a spinning drop in gyrostatic equilibrium. *Review of Scientific Instruments*, 48(12):1699–1705, 1977.

[34] Nature Technology Group. Introduction to produced water treatment. *Nature Technology Solution*, pages 2–18, 2005.

[35] S. Nave, J. Eastoe, R. K. Heenan, D. Steytler, and I. Grillo. What is so special about aerosol-ot? 2. microemulsion systems. *Langmuir*, 16(23):8741–8748, 2000.

[36] J. M. Neff. *Bioaccumulation in marine organisms: effect of contaminants from oil well produced water*. Elsevier, 2002.

[37] J. Y. Oldshue. *Fluid mixing technology*. McGraw-Hill, 1983.

[38] OSPAR. https://odims.ospar.org/documents/684. [Online; accessed 10-December-2017].

[39] J. Sjöblom, R. Lindberg, and S. E. Friberg. Microemulsionsphase equilibria characterization, structures, applications and chemical reactions. *Advances in colloid and interface science*, 65:125–287, 1996.

[40] J. Sleicher, C.A. Maximum stable drop size in turbulent flow. *AICHE Journal*, 8(4):471–477, 1962.

[41] J. Solsvik and H. A. Jakobsen. Single drop breakup experiments in stirred liquid-liquid tank. *Chemical Engineering Science*, 131:219–234, 2015.

[42] F. Sprow. Distribution of drop sizes produced in turbulent liquidliquid dispersion. *Chemical Engineering Science*, 22(3):435–442, 1967.

[43] G. B. Tatterson. *Fluid mixing and gas dispersion in agitated tanks*. McGraw-Hill Companies, 1991.

[44] G. T. Tellez, N. Nirmalakhandan, and J. L. Gardea-Torresdey. Performance evaluation of an activated sludge system for removing petroleum hydrocarbons from oilfield produced water. *Advances in Environmental Research*, 6(4):455–470, 2002.

[45] C. Tsouris and L. L. Tavlarides. Breakage and coalescence models for drops in turbulent dispersions. *AIChE Journal*, 40(3):395–406, 1994.

[46] USEPA. http://www.epa.gov. [Online; accessed 4-December-2017].

[47] N. Vankova, S. Tcholakova, N. D. Denkov, I. B. Ivanov, V. D. Vulchev, and T. Danner. Emulsification in turbulent flow. 1. Mean and maximum drop diameters in inertial and viscous regimes. *Journal of Colloid and Interface Science*, 312(2):363–380, 2007.

[48] N. Vankova, S. Tcholakova, N. D. Denkov, V. D. Vulchev, and T. Danner. Emulsification in turbulent flow. 2. Breakage rate constants. *Journal of Colloid and Interface Science*, 313(2):612–629, 2007.

[49] J. a. Veil. Comparison of Two International Approaches to Controlling Risk from Produced Water Discharges. 2008.

[50] J. A. Veil, M. G. Puder, D. Elcock, and R. J. Redweik Jr. A white paper describing produced water from production of crude oil, natural gas, and coal bed methane. *Department of Energy white paper*, (January):1–79, 2004.

[51] J. Viades-Trejo and J. Gracia-Fadrique. Spinning drop method: from young–laplace to vonnegut. *Colloids and Surfaces A: Physicochemical and Engineering Aspects*, 302(1-3):549–552, 2007.

[52] B. Vonnegut. Rotating bubble method for the determination of surface and interfacial tensions. *Review of scientific instruments*, 13(1):6–9, 1942.

[53] J. F. Walter and H. W. Blanch. Bubble break-up in gas-liquid bioreactors: Break-up in turbulent flows. *The Chemical Engineering Journal*, 32(1), 1986.

[54] C. Y. Wang and R. V. Calabrese. Drop breakup in turbulent stirred???tank contactors. Part II: Relative influence of viscosity and interfacial tension. *AIChE Journal*, 32(4):667–676, 1986.

[55] K. M. Wilkinson, C. D. Bain, H. Matsubara, and M. Aratono. Wetting of surfactant solutions by alkanes. *ChemPhysChem*, 6(3):547–555, 2005.